Umut Deniz Özugurel

Polynomial Preconditioning of the Dirac-Wilson Operator of the $\mathcal{N} = 1$ SU(2) Supersymmetric Yang-Mills Theory

2014

Theoretische Physik

Polynomial Preconditioning of the Dirac-Wilson Operator of the $\mathcal{N}=1$ SU(2) Supersymmetric Yang-Mills Theory

Inaugural-Dissertation
zur Erlangung des Doktorgrades
der Naturwissenschaften im Fachbereich Physik
der Mathematisch-Naturwissenschaftlichen Fakultät
der Westfälischen Wilhelms-Universität Münster

vorgelegt von
Umut Deniz Özugurel
aus Çorum/Türkei
-2014-

Dekan:	Prof. Dr. Christian Weinheimer
Erster Gutachter:	Prof. Dr. Gernot Münster
Zweiter Gutachter:	PD Dr. Jochen Heitger
Tag der mündlichen Prüfung:	30.01.2015
Tag der Promotion:	30.01.2015

Abstract

$\mathcal{N}$=1 SU(2) supersymmetric Yang-Mills theory has several interesting non-perturbative features that can be examined on a spacetime lattice by Monte Carlo simulations. This approach requires the introduction of sophisticated mathematical tools and novel techniques. One mathematical problem that needs particular attention is the emergence of a Pfaffian by the evaluation of the path integral over the Majorana field. This Pfaffian can have negative values, therefore it cannot be used as a measure for the importance sampling of the path integral over the gauge field. The solution is to use its magnitude as the measure and to reweight the obtained observable with its sign. Its sign can be determined by counting the two-fold degenerate pairs of negative real eigenvalues of the Dirac-Wilson operator. It is possible to obtain these eigenvalues by transforming the Dirac-Wilson operator by a polynomial before calculating a portion of its eigenspectrum using an iterative eigensolver. Power and Faber polynomials were studied in this context.

Contents

1. Introduction

Several problems in the Standard Model are solved by supersymmetry (SUSY) and several theories beyond the Standard Model have it as an indispensable ingredient. Therefore it is essential to study its properties. Even the simplest strongly coupled supersymmetric theory, namely the supersymmetric Yang-Mills theory with one supercharge ($\mathcal{N}$=1 SYM), has several important non-perturbative features, which are not completely understood. Among these are SUSY anomalies, confinement, spontaneous breaking of chiral symmetry and low-energy bound states. It is possible to study these by reformulating the theory on a spacetime lattice and calculating discretized functional integrals using numerical Monte Carlo techniques [1].

$\mathcal{N}$=1 SYM has only the gluon and the gluino as fields. Gauge invariance dictates that the gluino is a Majorana fermion in the adjoint representation of the gauge group. Its Majorana nature induces a Pfaffian instead of a determinant, as in the case of Dirac fermions, when the fermionic functional integral corresponding to the Green's function in consideration is evaluated. Since there are not any properties that prevent the Pfaffian to be negative, only its magnitude may be used as a factor in the weight function in the Monte Carlo technique that we are using. Its sign is used afterwards as a reweighting factor.

However a direct calculation of the Pfaffian is not possible with current computer technology on lattices large enough to provide realistic results. Its magnitude is approximated using pseudofermions. Its sign is obtained by counting the degenerate pairs of negative real eigenvalues of the Dirac-Wilson operator D of the lattice Lagrangian. This means that it is enough to calculate only the negative real eigenvalues. The standard method for this is the spectral flow method [2].

A much more efficient method for calculating negative real eigenvalues is to transform D by a polynomial and then using an iterative eigensolver to calculate only a part of the eigenspectrum of the new operator, which contains the transformed negative real eigenvalues. Power polynomials were already investigated in this context. Another class of polynomials, namely Faber polynomials, are introduced in this thesis. They were extensively studied in the context of iterative solvers of linear systems of equations due to their acceleration effect and in the context of numerical conformal mapping as a basis for approximating conformal mappings.

The outline of the thesis is the following. In chapter 2, the concept of supersymmetry is introduced in terms of its algebra and the constructions of the Lagrangian of $\mathcal{N}$=1 SYM and of the effective Lagrangians that predict the low-energy bound states are shortly explained. In chapter 3, the Curci-Veneziano action is derived and the solution to the consequent Pfaffian sign problem is shown. In chapter 4, the symmetries of the eigenspectrum of the Dirac-Wilson operator in the adjoint representation are summa-

rized. In chapter 5, the definition of Faber polynomials, the meaning of their optimality, their construction from two different exterior conformal maps and finally numerical experiments are presented. In chapter 6, latest published simulation results concerning the mass spectra of the bound state supermultiplets predicted by the effective theories and the effect of the finite volume of the lattice are summarized.

2. $\mathcal{N}$=1 SYM

Supersymmetry was developed in two different contexts, namely supergroups [3, 4] and string theory [5]. It mixes bosonic and fermionic fields and converts a boson state into a fermion and vice versa by supersymmetry generators Q_i. Q_i transform like spinors under the Lorentz group, therefore in 4 spacetime dimensions, Q_i must have at least 4 real components. $\mathcal{N}$=1 is the case where this minimal value is chosen, that is, where there is only one spinor operator Q with 4 components.

2.1. Supersymmetry Algebra

The supersymmetry algebra is Z_2-graded. The group of integers under addition is a very simple example with a Z_2-graded structure, which enables a simple explanation of the concept [6]. With e for even integer and o for odd integer, we have the following structure:

$$e + e = e \quad , \quad e + o = o \quad , \quad o + o = e \ , \tag{2.1}$$

with addition being the group product. The even numbers, with $\deg e = 0$, belong to the even subspace V_0 and the odd numbers, with $\deg o = 0$, belong to the odd subspace V_1, forming the group of integers by $V = V_0 \oplus V_1$.

Similarly, the supersymmetry generator Q belongs to the odd subspace and the Lorentz generators $M_{\mu\nu}$ and the translation generators P_μ to the even space, which is the Poincaré algebra [7]. The direct product of these two spaces is the Poincaré superalgebra with the commutation relations [4, 8]

$$[P^\mu, P^\nu] = 0 \tag{2.2}$$
$$[M^{\mu\nu}, P^\rho] = \mathrm{i}(\eta^{\nu\rho}P^\mu - \eta^{\mu\rho}P^\nu) \tag{2.3}$$
$$[M^{\mu\nu}, M^{\rho\sigma}] = \mathrm{i}(\eta^{\nu\rho}M^{\mu\sigma} + \eta^{\mu\sigma}M^{\nu\rho} - \eta^{\mu\rho}M^{\nu\sigma} - \eta^{\nu\sigma}M^{\mu\sigma}) \tag{2.4}$$
$$[P^\mu, Q_i] = 0 \tag{2.5}$$
$$[M^{\mu\nu}, Q_i] = \mathrm{i}(\sigma^{\mu\nu})_i Q_{ij} \tag{2.6}$$
$$\{Q_i, Q_j\} = (C\gamma_\mu)_{ij}P_\mu \ . \tag{2.7}$$

The corresponding Casimir operators are $P^2 = P_\mu P^\mu$ and $C^2 = C_{\mu\nu}C^{\mu\nu}$, with

$$C_{\mu\nu} = Y_\mu P_\nu - Y_\nu P_\mu \ , \tag{2.8}$$

where

$$Y^\mu = W^\mu - \frac{1}{4}Q\sigma^\mu\bar{Q} \ , \tag{2.9}$$

with Q the left-handed Weyl spinor, $\bar{Q}$ the right-handed Weyl spinor and W^μ the Pauli-Lubanski operator,

$$W_\mu = \frac{1}{2}\epsilon_{\mu\nu\rho\sigma}P^\nu M^{\rho\sigma} \ . \tag{2.10}$$

Their eigenvalues m^2 of P^2 and $2m^4y(y+1)$ of C^2, which are used for classifying the representation, reveal that SUSY multiplets, or supermultiplets, are degenerate in mass and contain an equal number of bosonic and fermionic degrees of freedom.

Two multiplets are relevant for $\mathcal{N}$=1 SYM, namely the massive chiral multiplet and the massless vector multiplet. The massive chiral multiplet is corresponds to the representation with the eigenvalues m and $y = 0$ and consists of a scalar field, a pseudoscalar field and a spinor. The massless vector multiplet is composed of a massless spin-1 boson with two helicity states and a massless spin-1/2 Weyl fermion again with two helicity states, like any other representation with $m = 0$ of the Poincaré superalgebra [4].

2.2. Lagrangian

The Lagrangian of $\mathcal{N}$=1 SYM is constructed from the massless vector multiplet, which consists of the gauge boson A_μ, that is, the gluon, and the two-component Weyl fermion ψ, that is, the gluino. A_μ is an element of the Lie algebra, so $A_\mu = A_\mu^a T^a$ where $T^a \in \mathrm{su}(3)$ and transforms in the adjoint representation of the group. This must hold also for ψ, therefore $\psi = \psi^a T^a$.

A_μ and ψ have the same number of on-shell degrees of freedom, two helicity states each. However, the number of their off-shell degrees of freedom differ. A_μ^a has 3 real bosonic degrees of freedom, whereas ψ^a has two comples, or 4 real, fermionic degrees of freedom. Therefore, one real bosonic auxiliary field, typically denoted D^a, is inserted. It is also an element of su(3). The Lagrangian for this vector multiplet is [9]

$$\mathcal{L} = -\frac{1}{4}F^a_{\mu\nu}F^{a,\mu\nu} + \mathrm{i}\psi^{\dagger\,a}\bar{\sigma}^\mu\mathcal{D}_\mu\psi^a + \frac{1}{2}D^aD^a \ , \tag{2.11}$$

where $\psi^{\dagger\,a}$ stands for a right-handed Weyl spinor, $\bar{\sigma}^0 = \sigma^0$ and $\bar{\sigma}^{1,2,3} = -\sigma^{1,2,3}$,

$$F^a_{\mu\nu} = \partial_\mu A^a_\nu - \partial_\nu A^a_\mu + g f^{abc} A^b_\mu A^c_\nu \tag{2.12}$$

is the Yang-Mills field strength tensor and

$$\mathcal{D}_\mu\psi^a = \partial_\mu\psi^a + g f^{abc} A^b_\mu \psi^c \tag{2.13}$$

is the covariant derivative in the adjoint representation.

The auxiliary field D^a has no kinetic term and is of dimension [mass]^2, so it can be eliminated by its equation of motion, which is algebraic. In terms of a Majorana spinor

$$\lambda = \begin{pmatrix} \psi \\ \psi^\dagger \end{pmatrix} \tag{2.14}$$

the Lagrangian takes the form

$$\mathcal{L} = -\frac{1}{4} F^a_{\mu\nu} F^{a,\mu\nu} + \mathrm{i}\,\bar{\lambda}^a \gamma^\mu \mathcal{D}^{ab}_\mu \lambda^b \ . \tag{2.15}$$

The Lagrangian must be represented in Euclidean spacetime for numerical simulation on the lattice. By making the substitution

$$t = -\mathrm{i}\tau \quad , \quad \tau \in \mathbb{R} \ , \tag{2.16}$$

so that time is imaginary and the metric is Euclidean, we get the Lagrangian in Euclidean spacetime [10]

$$\mathcal{L} = \frac{1}{4} F^a_{\mu\nu} F^a_{\mu\nu} + \frac{1}{2} \bar{\lambda}^a \gamma_\mu (D_\mu \lambda)^a + \frac{m_g}{2}\, \bar{\lambda}^a \lambda^a \ , \tag{2.17}$$

where in our case a soft symmetry breaking gluino mass m_g is inserted for technical reasons. The infinitesimal supersymmetry transformations of the fields with a Grassmannian parameter ϵ are

$$\delta A^a_\mu = 2\mathrm{i}\bar{\epsilon}\gamma_\mu \lambda^a \quad , \quad \delta\lambda^a = -\sigma_{\mu\nu} F^a_{\mu\nu} \epsilon \ . \tag{2.18}$$

The change in the Lagrangian is

$$\delta\mathcal{L} = \bar{\epsilon}\partial_\mu j_\mu \ , \tag{2.19}$$

where $j_\mu = -\frac{1}{2} S_\mu$ with S_μ the supercurrent defined as

$$S_\mu \equiv -F^a_{\rho\tau} \sigma_{\rho\tau} \gamma_\mu \lambda^a \ . \tag{2.20}$$

2.3. Effective Lagrangians

Two effective Lagrangian were proposed for $\mathcal{N}$=1 SYM to study its low energy behavior. They are written in terms of composite operators, which correspond to physical particles. The analysis of the first Lagrangian [11] predicts the formation of a massive chiral multiplet consisting of a Majorana fermion, a scalar boson and a pseudoscalar boson. The Majorana fermion is a bound state of a gluino and a gluon, hence called gluino-glue. The bosons are formed of two gluinos. The scalar one is named adjoint f_0 and the pseudoscalar one adjoint η'.

However, based on the Poincaré superalgebra, one expects also purely gluonic bound states, called glueballs [7]. In the first effective Lagrangian, they appear as auxiliary fields, therefore eliminated by their equation of motion. To include glueballs in the theory as dynamical fields, another effective Lagrangian [12] was constructed by embedding the chiral multiplet of the bound states with gluinos into a three-form multiplet [13]. The second chiral multiplet is consequently predicted. It consists of a scalar glueball, a pseudoscalar glueball and a gluino-glue.

Mixing between these two multiplets is also predicted, but it is unclear how significant that mixing might be and it is not clear which of them is lighter [14].

3. $\mathcal{N}$=1 SYM on the lattice

Calculations related to important properties such as confinement, mass spectrum of bound states, spontaneous symmetry breaking, in an asymptotically free theory like N=1 SYM are of non-perturbative nature. One suitable method is to reformulate the theory on a spacetime lattice, the distance between neighboring points of which is a, and calculate numerically functional integrals corresponding to Green functions of interest of this new theory.

3.1. Euclidean Functional Integral

The vacuum expectation value of an observable $\mathcal{O}$ for a gauge theory in Minkowski spacetime is in terms of a functional integral given by

$$\langle 0|\hat{\mathcal{O}}|0\rangle = \frac{1}{Z_M}\int(\mathfrak{D}A_\mu)(\mathfrak{D}\,\bar{\Psi})(\mathfrak{D}\Psi)\mathcal{O}[A_\mu,\bar{\Psi},\Psi]\mathrm{e}^{\mathrm{i}S_M[A_\mu,\bar{\Psi},\Psi]}\ , \tag{3.1}$$

with

$$Z_M = \int(\mathfrak{D}A_\mu)(\mathfrak{D}\,\bar{\Psi})(\mathfrak{D}\Psi)\mathrm{e}^{\mathrm{i}S_M[A_\mu,\bar{\Psi},\Psi]}\ , \tag{3.2}$$

where $S_M[A,\bar{\Psi},\Psi]$ the action of the theory, $\hat{\mathcal{O}}$ is the operator representing the observable, $\mathcal{O}[A,\bar{\Psi},\Psi]$ the functional representing the observable in terms of classical fields, namely A the gauge field, $\bar{\Psi}$ and Ψ the Grassmann-valued fermion fields.

In Euclidean spacetime, we have after applying (2.16)

$$\langle 0|\hat{\mathcal{O}}|0\rangle = \frac{1}{Z}\int(\mathfrak{D}A_\mu)(\mathfrak{D}\,\bar{\Psi})(\mathfrak{D}\Psi)\mathcal{O}[A_\mu,\bar{\Psi},\Psi]\mathrm{e}^{-S[A_\mu,\bar{\Psi},\Psi]}\ , \tag{3.3}$$

where

$$Z = \int(\mathfrak{D}A_\mu)(\mathfrak{D}\,\bar{\Psi})(\mathfrak{D}\Psi)\mathrm{e}^{-S[A_\mu,\bar{\Psi},\Psi]}\ , \tag{3.4}$$

with $S = -\mathrm{i}S_M$ being the Euclidean action. Since e^{-S} is a real number (with S in units of $\hbar$), the functional integral can be evaluated by reducing it to an ordinary multi-dimensional integral defined on a 4-dimensional spacetime lattice, which approximates Euclidean spacetime.

3.2. Wilson Action

The Lagrangian for a free quark of N colors in Euclidean spacetime is

$$\mathcal{L} = \bar{\Psi}(x)(\gamma_\mu\partial_\mu + m)\Psi(x)\ , \tag{3.5}$$

where γ_μ are the Euclidean Dirac matrices. A Lagrangian for interacting fermions is obtained by modifying (3.5) such that the new Lagrangian is invariant under the local gauge transformation

$$\Psi(x)' = \Lambda(x)\Psi(x), \;\; \Lambda(x) \in \mathrm{SU(N)} \; , \tag{3.6}$$

where

$$\Lambda(x) = \exp(\mathrm{i}\alpha_a(x)T^a), \;\; T^a \in \mathrm{su(N)} \; , \tag{3.7}$$

with su(N) being the Lie algebra of SU(N). This is achieved by making use of parallel transporters

$$U(y,x) = P \exp\left(\mathrm{i}\int_{\mathcal{C}_{yx}} A_\mu dx^\mu\right) \; , \tag{3.8}$$

where $\mathcal{C}_{yx}$ is some curve from x to y and $A_\mu = A_\mu^a T^a$ is the gauge field. Under (3.6), $U(y,x)$ transforms as

$$U'(y,x) = \Lambda(y)U(y,x)\Lambda(x)^\dagger \; . \tag{3.9}$$

Defining a covariant differential for an infinitesimal curve $\mathcal{C}_{x+dx,x}$ by

$$\mathcal{D}\Psi(x) = U(x+dx,x)^\dagger\Psi(x+dx) - \Psi(x) \; , \tag{3.10}$$

where

$$U(x+dx,x) = 1 + \mathrm{i}A_\mu(x)dx^\mu \; , \tag{3.11}$$

we obtain the covariant derivative

$$\mathcal{D}_\mu\Psi(x) = (\partial_\mu + \mathrm{i}A_\mu(x))\Psi(x) \; . \tag{3.12}$$

Replacing ∂_μ in (3.5) with (3.12), we obtain the locally gauge invariant Lagrangian for interacting fermions,

$$\mathcal{L} = \bar{\Psi}(x)(\gamma_\mu\mathcal{D}_\mu + m)\Psi(x) \; . \tag{3.13}$$

The corresponding action is

$$S[\bar{\Psi},\Psi,A] = \int d\tau \int d^3x\, \bar{\Psi}(x)(\gamma_\mu\mathcal{D}_\mu + m)\Psi(x) \; . \tag{3.14}$$

On a spacetime lattice, Ψ_x is defined at discrete points $x = an$, where a is distance between lattice points and $n \equiv (n_1,n_2,n_3,n_4)$ labels lattice points. Partial derivatives are replaced by the forward difference operator,

$$\partial_\mu \quad \to \quad \Delta_\mu^{\mathrm{f}} \equiv \frac{1}{a}\left(\Psi_{x+\hat{\mu}} - \Psi_x\right) \; , \tag{3.15}$$

and integrals by sums,

$$\int d^4 \quad \to \quad \sum_n a^4 \; . \tag{3.16}$$

Local gauge invariance of the action in this new setup is ensured the same way as in the continuum, that is, by replacing the lattice derivative (3.15) by the forward lattice covariant derivative

$$\mathrm{D}^{\mathrm{f}}_{\mu}\Psi_x = \frac{1}{a}(U^{\dagger}_{x\mu}\Psi_{x+\hat{\mu}} - \Psi_x) \ , \tag{3.17}$$

with $U_{x\mu} \equiv U(x+\hat{\mu}, x)$. The curve connecting two neighbouring lattice points can be approximated by a straight line for small a, therefore

$$U_{x\mu} = \exp\left(\mathrm{i}aA_{x\mu}\right) \ , \tag{3.18}$$

which is an element of SU(N) and which we call a link from now on. The fermionic lattice action thus reads

$$S_F[\bar{\Psi}, \Psi, U] = \frac{a^4}{2}\sum_x \bar{\Psi}_x\,\gamma_\mu(\mathrm{D}^{\mathrm{f}}_{\mu} + \mathrm{D}^{\mathrm{b}}_{\mu})\Psi_x - m\,\bar{\Psi}_x\,\Psi_x \ , \tag{3.19}$$

where the backward lattice covariant derivative

$$\mathrm{D}^{\mathrm{b}}_{\mu}\Psi_x = \frac{1}{a}(\Psi_x - U^{\dagger}_{x-\hat{\mu},\mu}\Psi_{x-\hat{\mu}}) \tag{3.20}$$

is introduced to decrease discretization errors. Explicitely

$$S_F[\bar{\Psi}, \Psi, U] = a^4\sum_x \bar{\Psi}_x \sum_{\mu=1}^{4}\frac{\gamma_\mu}{2a}[U_{x\mu}\Psi_{x+\hat{\mu}} - U^{\dagger}_{x-\hat{\mu},\mu}\Psi_{x-\hat{\mu}}] - m\,\bar{\Psi}_x\,\Psi_x \ . \tag{3.21}$$

The gluonic action is constructed out of link variables, which represent gauge fields on the lattice. (3.9) implies that there are two gauge invariant objects possible. We present them in continuum notation to avoid clutter of indices. The first one is

$$\bar{\Psi}(x_i)P[U]\Psi(x_f) \ , \tag{3.22}$$

where, with $x_f - \hat{\mu}_{k-1} = x_i + \hat{\mu}_0 + \hat{\mu}_1 + \cdots + \hat{\mu}_{k-2}$,

$$P[U] = U_{\mu_0}(x_i)\,U_{\mu_1}(x_i+\hat{\mu}_0)\,U_{\mu_2}(x_i+\hat{\mu}_0+\hat{\mu}_1)\ldots U_{\mu_{k-1}}(x_f-\hat{\mu}_{k-1}) \ , \tag{3.23}$$

which, due to (3.9), transform as

$$P'[U] = \Lambda(x_i)P[U]\Lambda(x_f)^{\dagger} \ . \tag{3.24}$$

The second one is

$$L[U] = \mathrm{tr}[P_{\mathcal{C}}[U]] \ , \tag{3.25}$$

where $P_{\mathcal{C}}[U]$ is obtained by setting $x = x_i = x_f$ in (3.23). Under (3.9), $P_{\mathcal{C}}[U]$ transforms as

$$P'_{\mathcal{C}}[U] = \Lambda(x)P_{\mathcal{C}}[U]\Lambda(x)^{\dagger}, \tag{3.26}$$

which is a similarity transformation leaving the trace of $P_{\mathcal{C}}[U]$ invariant.

The smallest possible closed loop,

$$P_{x,\mu\nu} = U_{x\mu} U_{x+\hat{\mu},\nu} U^{\dagger}_{x+\hat{\nu},\mu} U^{\dagger}_{x\nu} \ , \tag{3.27}$$

is called plaquette and it is the building block of the lattice gauge action. Its expansion

$$\begin{aligned} P_{x,\mu\nu} &= \exp\left(ia^2(\partial_\mu A_\nu(x) - \partial_\nu A_\mu(x) + i[A_\mu(x), A_\nu(x)] + \mathcal{O}(a^3)\right) \\ &= \exp\left(ia^2 F_{\mu\nu}(x) + \mathcal{O}(a^3)\right) \end{aligned} \tag{3.28}$$

reveals that a lattice gauge action of the form

$$S_G[U] = \beta \sum_x \sum_{\mu<\nu} 1 - \mathrm{Re}\ \mathrm{tr}\, P_{x,\mu\nu} \ , \tag{3.29}$$

with $\beta = 2N/g^2$ and where the trace runs over the group indices, converges as $a \to 0$ to the continuum gauge action in the Euclidean space

$$S_G[A] = \frac{1}{2g^2}\ \mathrm{tr} \int d^4x F_{\mu\nu}(x) F_{\mu\nu}(x) \tag{3.30}$$

or, since $F_{\mu\nu} = F^a_{\mu\nu} T^a$ and $2\,\mathrm{tr}(T^a T^b) = \delta^{ab}$,

$$S_G[A] = \frac{1}{4g^2} \int d^4x F^a_{\mu\nu}(x) F^a_{\mu\nu}(x) \ . \tag{3.31}$$

The lattice fermion propagator in momentum space obtained for free fermions ($U_{x\mu} = 1$),

$$\frac{[-\mathrm{i}a^{-1}\gamma_\mu \sin(p_\mu a) + m]_{\alpha\beta}}{a^{-2}\sin^2(p_\mu a) + m^2} \tag{3.32}$$

has 16 poles when $m = 0$, which implies the existence of 15 additional fermions, which are pure lattice artifacts. One way to resolve this problem is to modify the action (3.21) such that the masses of the additional fermions diverge in the continuum limit. To this aim, chiral symmetry, which is a symmetry of (3.13), is abandoned by adding a term to the action (3.21):

$$S_F \quad \to \quad S_F - \frac{ar}{2} \sum_x \bar{\Psi}_x \Delta^{\mathrm{f}}_\mu \Delta^{\mathrm{b}}_\mu \Psi_x \tag{3.33}$$

and thus rendering (3.32) dependent on p as

$$m(p) = m + \frac{2r}{a} \sum_\mu \sin^2(p_\mu a/2). \tag{3.34}$$

This modification solves the doubling problem, but breaks the chiral symmetry, which would protect the mass against additive renormalization. Therefore the bare fermion mass m must be tuned appropriately.

The final form of the action is after reintroducing the gauge field,

$$S = a^4 \sum_x \left(m + \frac{4}{a}\right) \bar{\Psi}_x \Psi_x - \frac{1}{2a} \sum_{\mu=1}^{4} \left(\bar{\Psi}_{x+\hat{\mu}} U_{x\mu}(1+\gamma_\mu)\Psi_x - \bar{\Psi}_{x-\hat{\mu}} U^{\dagger}_{x-\hat{\mu},\mu}(1-\gamma_\mu)\Psi_x\right) \ , \tag{3.35}$$

where conventionally $r = 1$. Choosing for the fermion fields the normalization

$$a^{3/2}(am + 4r)^{1/2}\Psi_x \quad \rightarrow \quad \Psi_x \ , \tag{3.36}$$

we get

$$S = \sum_x \bar{\Psi}_x \, \Psi_x - \kappa \sum_{\mu=1}^{4} \left(\bar{\Psi}_{x+\hat{\mu}} \, U_{x\mu}(1+\gamma_\mu)\Psi_x - \bar{\Psi}_{x-\hat{\mu}} \, U^\dagger_{x-\hat{\mu},\mu}(1-\gamma_\mu)\Psi_x \right) \ , \tag{3.37}$$

where

$$\kappa = \frac{1}{2am + 8} \ . \tag{3.38}$$

3.3. Curci-Veneziano Action

One way to derive an action for Majorana fermions is to rewrite the action (3.37) in the adjoint representation and to express the adjoint Dirac fermions in terms of two adjoint Majorana fermions [10]. One could construct the theory without referring to Dirac fermions at all, but the approach described here enables us to use our existing numerical tools. The relation between the Pfaffian and the determinant of a matrix is also automatically proven.

The action for an adjoint Dirac fermion Ψ is

$$S_f[\bar{\Psi}, \Psi, V] = \sum_x \left(\bar{\Psi}_x \, \Psi_x - \kappa \sum_{\mu=1}^{4} \bar{\Psi}_{x+\hat{\mu}} \, V_{x\mu}(1+\gamma_\mu)\Psi_x + \bar{\Psi}_x \, V^T_{x\mu}(1-\gamma_\mu)\Psi_{x+\hat{\mu}} \right) \ , \tag{3.39}$$

where now $\Psi = \Psi^a T^a$ and

$$V^{ab}_\mu(x) = 2 \ \mathrm{tr}[U^\dagger_{x\mu} T^a U_{x\mu} T^b] \ . \tag{3.40}$$

The fermion must be massive in order that D is invertible, which is required in numerical calculations.

The adjoint Majorana fermions are

$$\lambda^1 \equiv \frac{1}{\sqrt{2}}(\Psi + C \, \bar{\Psi}^T) \ , \quad \lambda^2 \equiv \frac{\mathrm{i}}{\sqrt{2}}(-\Psi + C \, \bar{\Psi}^T) \ , \tag{3.41}$$

and they fulfill the Majorana condition

$$\lambda_c \equiv C \, \bar{\lambda}^T = \lambda \tag{3.42}$$

with C the charge conjugation matrix. Then the Dirac fermion and its charge conjugate are

$$\Psi = \frac{1}{\sqrt{2}}(\lambda^1 + \mathrm{i}\lambda^2), \qquad \Psi_c \equiv C\bar{\Psi}^T = \frac{1}{\sqrt{2}}(\lambda^1 - \mathrm{i}\lambda^2) \ . \tag{3.43}$$

When these are inserted into (3.39), we get in terms of 2 Majorana fields

$$S_f = \sum_{x,y} \bar{\Psi}^{\,i}_x \,\mathrm{D}\, \Psi^i_y = \frac{1}{2}\sum_{i=1}^{2}\sum_{x,y} \bar{\lambda}^{\,i}_x \,\mathrm{D}\, \lambda^i_y = \frac{1}{2}\sum_{i=1}^{2}\sum_{x,y} \lambda^i_x M \lambda^i_y \tag{3.44}$$

where $M \equiv C\,\mathrm{D}$ is an antisymmetric matrix and D is the Wilson-Dirac operator in the adjoint representation:

$$\mathrm{D}^{ab}_{xy} \equiv \delta_{xy}\delta^{ab} - \kappa \sum_{\mu=1}^{4} \Big(\delta_{x,y+\hat{\mu}} V^{ab}_{y\mu}(1+\gamma_\mu) + \delta_{x+\hat{\mu},y}(V^T_{x\mu})^{ab}(1-\gamma_\mu) \Big) \ . \tag{3.45}$$

Dropping one of the two Majorana fermions, one finally gets the Curci-Veneziano action, which consists of the usual gauge field action for the gluon and the fermionic action for the gluino in the adjoint representation of the gauge group $SU(2)$:

$$S = \beta \sum_x \sum_{\mu<\nu} (1 - \mathrm{Re}\ \mathrm{tr}\, P_{x,\mu\nu}) + \frac{1}{2}\sum_{x,y} \lambda_x M \lambda_y \ . \tag{3.46}$$

3.4. Discrete Functional Integral

The discrete functional integral is of the form

$$\langle \mathcal{O} \rangle = \frac{1}{Z} \int [d\lambda dV] \mathcal{O}[V, \bar{\lambda}, \lambda] \mathrm{e}^{-S_g[V] - \frac{1}{2}\lambda M \lambda} \tag{3.47}$$

where

$$Z = \int [d\lambda dV] \mathrm{e}^{-S_g[V] - \frac{1}{2}\lambda M \lambda} \tag{3.48}$$

with the measure

$$[d\lambda dV] \equiv \prod_x d\lambda_x \prod_\mu dV_{x\mu} \ , \tag{3.49}$$

where dV is the Haar measure. Note that this is an ordinary integral over Grassmann numbers and group elements.

We have the relation

$$\int [d\lambda] \exp\Big(-\frac{1}{2}\lambda M \lambda \Big) = \mathrm{Pf}(M) \ , \tag{3.50}$$

because the evaluation of the Gaussian integral yields the definition of the Pfaffian, which is

$$\mathrm{Pf}(A) \equiv \frac{1}{n!\, 2^n}\, \epsilon_{i_1 j_1 \cdots i_n j_n} A_{i_1 j_1} \cdots A_{i_n j_n} \ , \tag{3.51}$$

where A is a $2n \times 2n$ antisymmetic matrix and ϵ the permutation tensor. Similarly, we have the relation

$$\int [d\,\bar{\Psi}\, d\Psi] \exp\Big(-\,\bar{\Psi}\,\mathrm{D}\,\Psi \Big) = \det(\mathrm{D}) \ . \tag{3.52}$$

Due to (3.44) we obtain the following relation between the Pfaffian and the determinant:

$$\begin{aligned}\int [d\lambda^i] \exp\left(-\frac{1}{2}\sum_{i=1}^{2} \lambda^i M \lambda^i\right) &= \prod_{i=1}^{2} \int [d\lambda^i] \exp\left(-\frac{1}{2}\lambda^i M \lambda^i\right) \\ &= \mathrm{Pf}^2(M) \\ &= \det(\mathrm{D}) \ .\end{aligned} \tag{3.53}$$

The relation

$$\det(\gamma_5 \, \mathrm{D}) = \det(\gamma_5) \det(\mathrm{D}) = \det(\mathrm{D}) \tag{3.54}$$

implies that $\det(\mathrm{D})$ is always real, because $\det(\gamma_5 \, \mathrm{D})$, where $\gamma_5 \, \mathrm{D}$ is the Hermitian Wilson-Dirac operator, is always real. Moreover $\det(\mathrm{D})$ is always positive due to the two-fold degeneracy of its eigenvalues, as proven in the next chapter. Therefore due to (3.53) $\mathrm{Pf}(M)$ does not have to be positive.

Evaluating (3.47) we get

$$\langle \mathcal{O} \rangle = \frac{\int [dV] \, \tilde{\mathcal{O}}[V, \mathrm{D}^{-1}[V]] \, \mathrm{e}^{-S_g} \, \mathrm{Pf}(M[V])}{\int [dV] \, \mathrm{e}^{-S_g} \, \mathrm{Pf}(M[V])} \ , \tag{3.55}$$

where $\tilde{\mathcal{O}}[V, \mathrm{D}^{-1}[V]]$ is obtained from $\mathcal{O}[V, \bar{\lambda}, \lambda]$ by replacing each $\lambda \, \bar{\lambda}$ pair by $\mathrm{D}^{-1}[V]$ after Wick's contraction. This last expression can be rewritten with an effective action $S_{\mathrm{eff}} = S_g - \ln(\mathrm{Pf}(M[V]))$ as

$$\langle \mathcal{O} \rangle = \frac{\int [dV] \, \tilde{\mathcal{O}}[V, \mathrm{D}^{-1}[V]] \, \mathrm{e}^{-S_{\mathrm{eff}}}}{\int [dV] \, \mathrm{e}^{-S_{\mathrm{eff}}}} \ . \tag{3.56}$$

Since M is always invertible, $\ln(\mathrm{Pf}(M))$ is always finite, but it can be complex, because $\mathrm{Pf}(M)$ can be negative. Since a complex S_{eff} cannot be used as a measure for importance sampling of (3.47), $|\,\mathrm{Pf}(M)|$ is replaced by $(\det(M))^{1/2}$ and so

$$\mathrm{S}^{\mathrm{R}}_{\mathrm{eff}} = S_g - \frac{1}{2} \ln(\det(\mathrm{D}[V])) \tag{3.57}$$

is used and the omitted sign is taken into account in the following way:

$$\begin{aligned}\langle \mathcal{O} \rangle &= \frac{\int [dV] \, \mathrm{e}^{-\,\mathrm{S}^{\mathrm{R}}_{\mathrm{eff}}} [\mathrm{sgn}(\mathrm{Pf}(M[V])) \, \tilde{\mathcal{O}}]}{\int [dV] \, \mathrm{e}^{-\,\mathrm{S}^{\mathrm{R}}_{\mathrm{eff}}}} \, \frac{\int [dV] \, \mathrm{e}^{-\,\mathrm{S}^{\mathrm{R}}_{\mathrm{eff}}}}{\int [dV] \, \mathrm{e}^{-\,\mathrm{S}^{\mathrm{R}}_{\mathrm{eff}}} [\mathrm{sgn}(\mathrm{Pf}(M[V]))]} \\ &= \frac{\langle \mathrm{sgn}(\mathrm{Pf}(M[V])) \, \tilde{\mathcal{O}} \rangle_{\mathrm{R}}}{\langle \mathrm{sgn}(\mathrm{Pf}(M[V])) \rangle_{\mathrm{R}}} \ .\end{aligned} \tag{3.58}$$

An exact calculation of $\mathrm{Pf}(M)$ is unfeasible with current computing power, therefore its magnitude $|\,\mathrm{Pf}(M)|$ is expressed as a functional integral over complex bosonic fields ϕ called pseudofermions as

$$|\,\mathrm{Pf}(M)| = \det(\mathrm{D})^{1/2} = (\det(\mathrm{D}^\dagger \, \mathrm{D}))^{1/4} = \int [d\phi^\dagger \, d\phi] \exp\left(\phi^\dagger \, (\mathrm{D}^\dagger \, \mathrm{D})^{-1/4} \, \phi\right) \tag{3.59}$$

and $(\mathrm{D}^\dagger \mathrm{D})^{-1/4}$ is approximated by a polynomial $P(\mathrm{D}^\dagger \mathrm{D})$ if importance sampling is done using Polynomial Hybrid Monte Carlo or by a rational function if Rational Hybrid Monte Carlo is used.

Defining $\mathcal{O}^{\mathrm{s}} \equiv \mathrm{sgn}(\mathrm{Pf}(M))\,\tilde{\mathcal{O}}$ and $\mathfrak{S} \equiv \mathrm{sgn}(\mathrm{Pf}(M))$, the vacuum expectation value is then approximated by

$$\langle \mathcal{O} \rangle \simeq \frac{\sum_i \mathcal{O}_i^{\mathrm{s}}}{\sum_i \mathfrak{S}_i} \ , \tag{3.60}$$

where $\mathcal{O}_i^{\mathrm{s}}$ and $\mathfrak{S}_i$ are the values of the observables calculated with the ith element C_i of the configuration set generated by the importance sampling algorithm in use. C_i is itself also a set of links $U_{x\mu}$ defining the configuration of the system.

3.5. Continuum Limit

The action (3.46) is based on abandoning the idea of maintaining supersymmetry on the lattice. Supersymmetry is recovered simultaneously with chiral symmetry in the continuum limit by tuning the bare gluino mass m, hence κ, to a critical value such that the renormalized gluino mass vanishes. The chiral symmetry, or the axial symmetry $U(1)_A$, is not explicitly broken to any order in perturbation theory. However it is at the non-perturbative level anomalously broken to the discrete subgroup Z_{2N}, which is further spontaneously broken to Z_2.

It is explicitly shown by chiral perturbation theory in a partially quenched scheme that

$$m_{a-\pi}^2 \propto m_g \ , \tag{3.61}$$

where $m_{a-\pi}$ is the mass of the (unphysical) adjoint pion mass and m_g the renormalized gluino mass. Critical κ, noted by κ_c, which corresponds to chiral limit, is then obtained by extrapolating the linear fit of different values of $1/\kappa$ versus $m_{a-\pi}^2$ to the point where $m_{a-\pi}$ vanishes.

4. Eigenspectrum of the Dirac-Wilson Operator

The continuous Dirac operator D_c in the massless limit is anti-hermitian, that is, it has only imaginary and zero eigenvalues. It is therefore a normal operator, that is $[\mathrm{D}_c, \mathrm{D}_c^\dagger] = 0$. Moreover it has γ_5-hermiticity, that is, $\gamma_5 \, \mathrm{D}_c \, \gamma_5 = \mathrm{D}_c^\dagger$. The mass shifts the origin to its value. This property is absent for the discrete Dirac-Wilson operator. And it looses its normality, so its eigenvectors not need be orthogonal. But the γ_5-hermiticity and therefore the complex pairing of eigenvalues mentioned below are maintained.

D is diagonalizable, that is, $V^{-1} \, \mathrm{D} \, V = \Lambda$. V is of the dimensions of D and its columns are linearly independent. Λ is a diagonal matrix of the dimensions of D and its diagonal elements are the eigenvalues of D. When a right eigenvector v_i is defined as

$$\mathrm{D} \, v_i = \lambda_i v_i \tag{4.1}$$

and a left eigenvector $u_i^\dagger$ as

$$u_i^\dagger \, \mathrm{D} = \lambda_i u_i^\dagger \ , \tag{4.2}$$

then each column of V corresponds to a v_i and each row of V^{-1} to a $u_i^\dagger$. Since $V^{-1} V = I$ by definition,

$$u_i^\dagger v_j = \delta_{ij} \ . \tag{4.3}$$

There are three useful similarity transformations for the the adjoint representation of D. The first one is

$$\mathrm{D}^\top = C \, \mathrm{D} \, C^{-1} \ . \tag{4.4}$$

We then have

$$\mathrm{D}^\top \, w = \lambda w \quad \Leftrightarrow \quad \mathrm{D}^\dagger \, w^* = \lambda^* w^* \ , \quad w \equiv Cv \ . \tag{4.5}$$

which means

$$u_i^\dagger = (C v_i)^\top \ . \tag{4.6}$$

But $(C v_i)^\top v_i = 0$ as opposed to (4.3) since

$$(C v_i)^\top v_i = v_i^\top C^\top v_i = (v_i^\top C^\top v_i)^\top = v_i^\top C v_i = -v_i^\top C^\top v_i \ . \tag{4.7}$$

Therefore there exist another left eigenvector for λ_i, which means D is at least doubly degenerate.

The second similarity transformation

$$\mathrm{D}^\dagger = \gamma_5 \, \mathrm{D} \, \gamma_5 \tag{4.8}$$

results in

$$\mathrm{D}^\dagger w = \lambda w \ , \quad w \equiv \gamma_5 v \ , \tag{4.9}$$

which means

$$u_j^\dagger = (\gamma_5 v_i)^\dagger \ , \tag{4.10}$$

with $\lambda_j = \lambda_i^*$.

By establishing a relation between the right eigenvector of λ and the left eigenvector of λ^*, we conclude that each eigenvalue has a complex partner, that is, the eigenspectrum of D is symmetric with respect to the real axis of its complex plane.

Using these two relations we get the third similarity transformation

$$\mathrm{D}^* = B\,\mathrm{D}\,B^{-1} \tag{4.11}$$

and

$$\mathrm{D}^* w = \lambda w \quad \Leftrightarrow \quad \mathrm{D}\, w^* = \lambda^* w^* \ , \quad w \equiv Bv \ , \tag{4.12}$$

with $B = C\,\gamma_5$. Therefore

$$v_j = C\,\gamma_5\, v_i^* \ , \tag{4.13}$$

with $\lambda_j = \lambda_i^*$.

These relations allow us to introduce the Hermitian matrix $\tilde{\mathrm{D}} \equiv \gamma_5\,\mathrm{D}$ and the anti-symmetric matrix $M \equiv C\,\mathrm{D}$.

The definition (3.45) of D can be rewritten by representing the summation in the second term by a matrix, denoted H, as

$$\mathrm{D} = 1 - \kappa H \ . \tag{4.14}$$

H is called the hopping matrix. It has the similarity transformation

$$OHO = -H \ , \tag{4.15}$$

where $O_{xy} = (-1)^{(x_1+x_2+x_3+x_4)}\delta_{xy}$, implies [15] that the eigenspectrum of H is invariant under sign change, therefore the eigenspectrum of D is symmetric with respect to the line $z = 1$.

Eigenspectra at a fixed lattice spacing, but at two different volumes are shown in figure 4.1. One can see the holes in the spectrum due to fermion doubling. One also sees that the eigenspectrum covers the same region in the complex plane at larger volume, but it is denser. This is related to the fact that a differential operator, which has a continuous spectrum in the whole space, has in finite space a discrete spectrum with a fixed boundary, whose density increases with the extent of the space.

Figure 4.2 shows how the value of κ effects the size of the region the eigenspectrum of D covers. It is a factor before H, so increasing it enlarges the eigenspectrum of D, which causes eigenvalues enter left half-plane.

For numerical purposes, D can be brought to the form

$$\hat{\mathrm{D}} = 1 - \kappa^2 \begin{pmatrix} 0 & 0 \\ 0 & \mathrm{D}_{oe}\,\mathrm{D}_{eo} \end{pmatrix} \ , \tag{4.16}$$

where D_{eo} is the matrix formed of elements of D, the sum of the indices of which is even, and D_{oe} is the odd counterpart. Then, the eigenvalues λ_p of $\hat{\mathrm{D}}$ is related to the eigenvalues λ of D by [15]

$$\lambda_p = \lambda(2 - \lambda) \ . \tag{4.17}$$

This rearrangement of the element of D is called even-odd preconditioning. Preconditioning means in this context means changing the condition number of a matrix, which is the ratio of the largest to smallest singular value of that matrix. Its effect on the eigenspectrum is illustrated in figure 4.3. The eigenspectrum of $\hat{\mathrm{D}}$ covers a smaller region on the complex plane and the smaller eigenvalues of D are mapped away to the imaginary axis. Tis implies that $\hat{\mathrm{D}}$ has a smaller condition number than D. It has also half as many eigenvalues. All these effects result in a faster numerical calculation of eigenvalues.

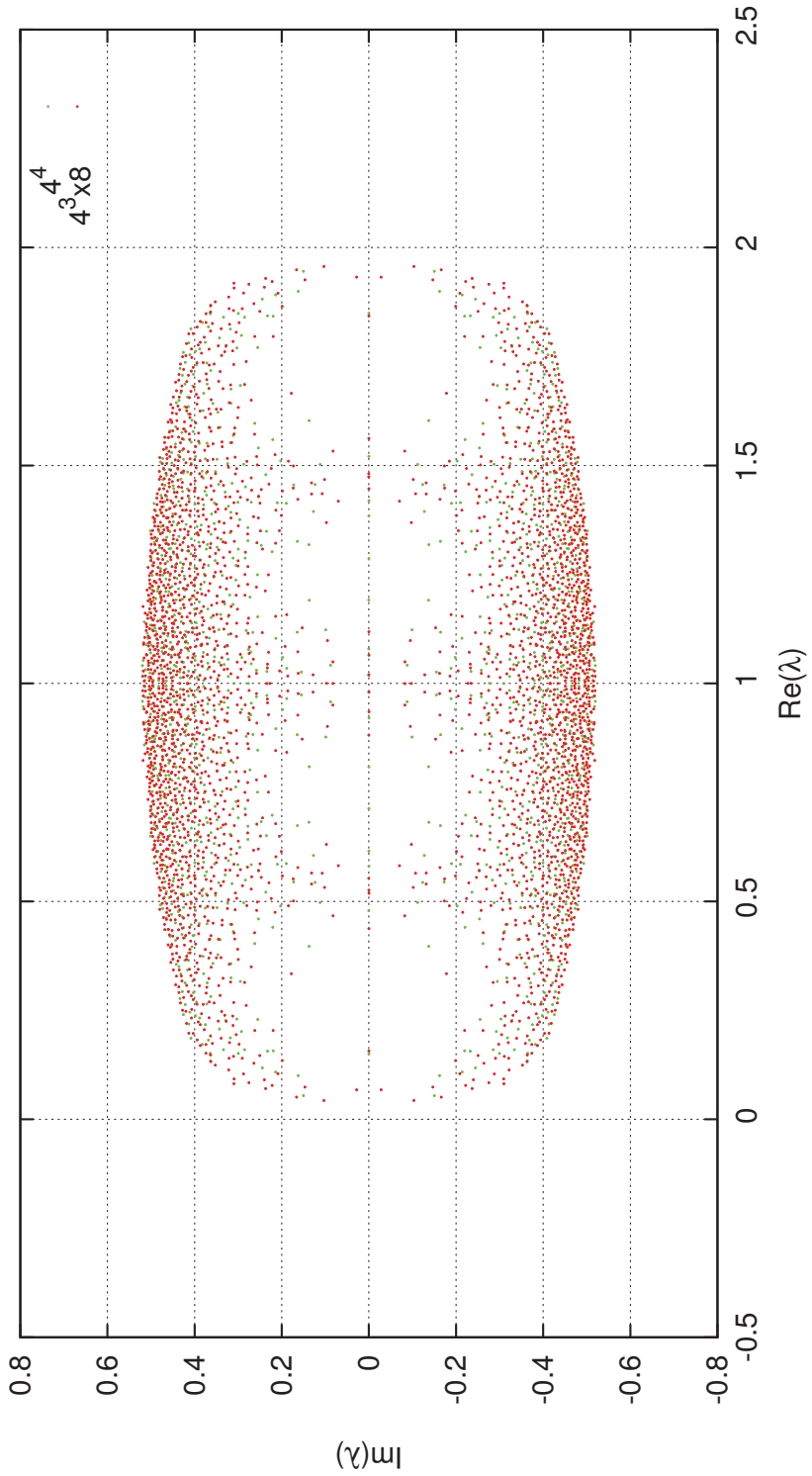

Figure 4.1.: Eigenspectra at two different volumes at $\beta = 1.60$ and $\kappa = 0.1570$. The eigenspectrum corresponding to the larger lattice (red dots) is denser than the other.

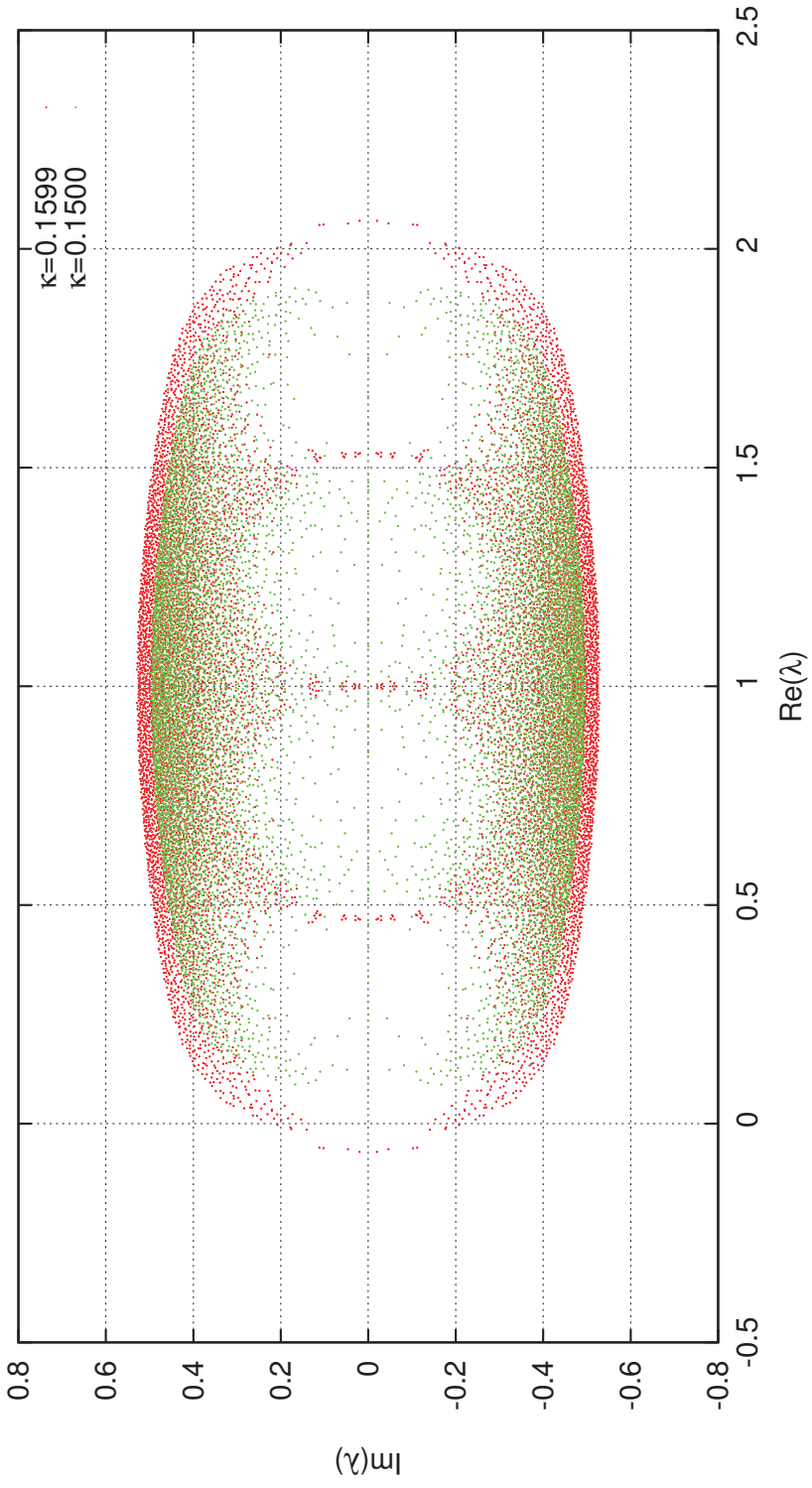

Figure 4.2.: Eigenspectra at two different values of κ on a lattice of volume $6^3 \times 8$

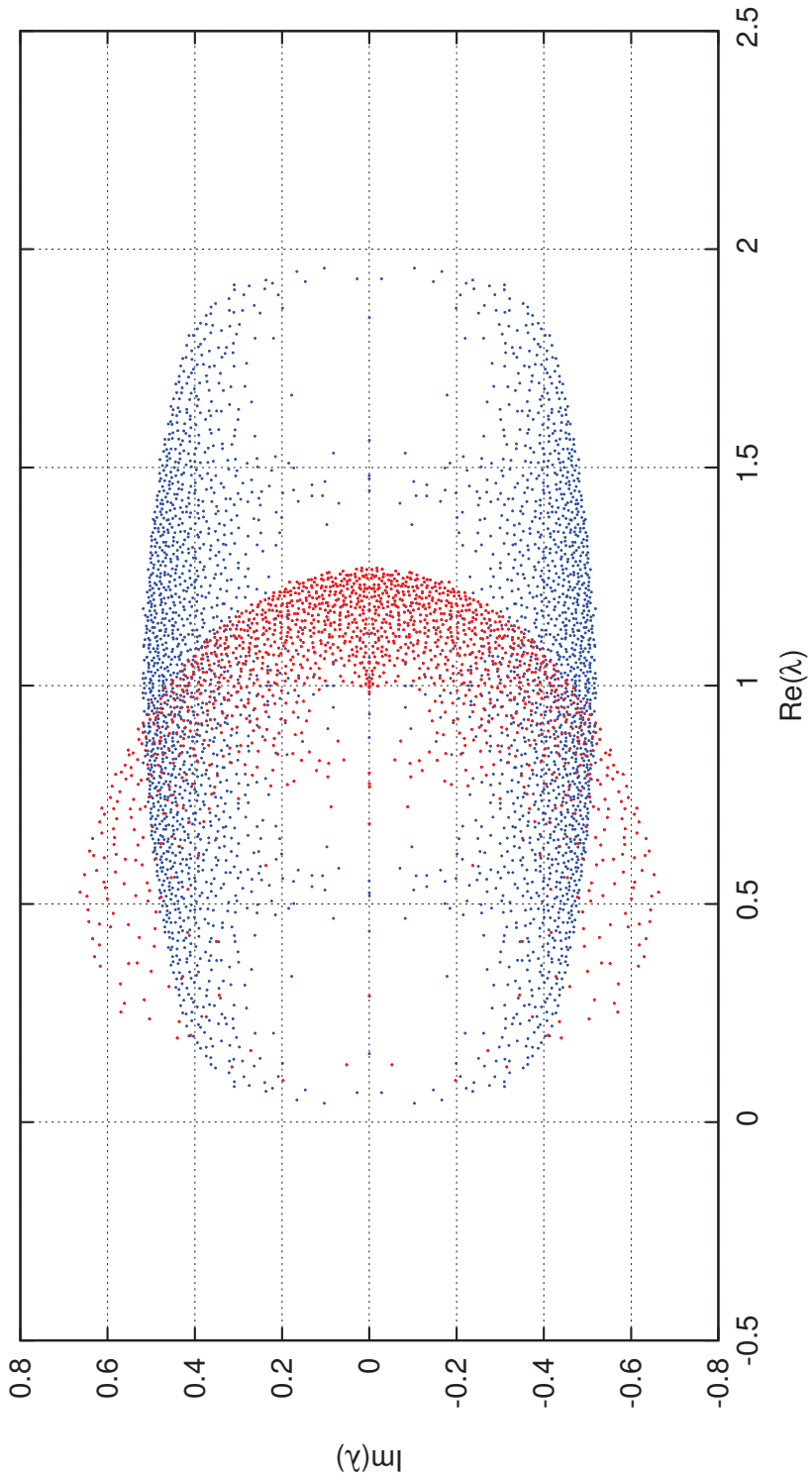

Figure 4.3.: Eigenspectra of D (blue dots) and of $\hat{\mathrm{D}}$ on a lattice of volume $4^3 \times 8$ at $\beta = 1.60$ and $\kappa = 0.1570$

5. Polynomial Filtering of Eigenvalues

A direct calculation of $\mathrm{Pf}(M)$ is unfeasible due to technical limitations. Storage of D needs too much memory, around 10PB in double precision for a lattice of volume $32^3 \times 64$ with SU(2). Even if it could be stored, its computation time would be prohibitively long, even though D is sparse, that is, most of its elements are 0. Therefore $|\mathrm{Pf}(M)|$ is approximated as mentioned in chapter 3 and $\mathrm{sgn}(\mathrm{Pf}(M))$ is obtained separately by counting the degenerate real negative eigenvalue pairs of D [16].

The direct method to calculate the negative real eigenvalues is to diagonalize D. However this is not possible because of the same limitations that prevent us to directly calculate $\mathrm{Pf}(M)$. Therefore we use an iterative eigensolver for non-normal matrices, namely ARPACK [17], which is a Fortran implementation of the Arnoldi algorithm [18]. Although this eigensolver allows us to obtain an arbitrary number of eigenvalues, time that it needs to calculate all the negative real eigenvalues is very long because of the other complex eigenvalues with a negative imaginary part.

The standard method to calculate real eigenvalues is to use the spectral flow method [2, 19]. In this method the real eigenvalues of D are obtained, noting that ${\gamma_5}^2 = 1$, by

$$\gamma_5(\mathrm{D}-\sigma)v = 0 \quad \Rightarrow \quad (\mathrm{D}-\sigma)v = 0 \quad \Leftrightarrow \quad \mathrm{D}\,v = \sigma v \quad , \quad \sigma \in \mathbb{R}\ , \tag{5.1}$$

where $\gamma_5\,\mathrm{D}$ is the Hermitian Dirac-Wilson operator, σ some shift and v is the eigenvector corresponding to the eigenvalue 0.

The fact that iterative eigensolvers calculate an arbitrary number of eigenvalues allows us to introduce another much more efficient method. It is to precondition D by a polynomial, that is, apply a polynomial on D so that real negative eigenvalues are calculated before the other ones in the iteration (see [20] for an extensive review on iterative solvers). The eigenvectors of D remains unchanged by the preconditioning because for a polynomial P of order n and with coefficients α_k, we have

$$P(\mathrm{D})v_i = \sum_{k=0}^{n} \alpha_k (\mathrm{D})^k v_i = \sum_{k=0}^{n} \alpha_k \lambda_i^k v_i = P(\lambda_i) v_i\ , \tag{5.2}$$

where v_i are the eigenvectors of D and λ_i the corresponding eigenvalues. Iterative eigensolvers calculate eigenvectors along with eigenvalues. Since D and $P(\mathrm{D})$ share the same eigenvectors, eigenvalues of D can be easily obtained from them.

Figures 5.1-5.4 illustrate the idea. In figure 5.1, the eigenspectrum of a random matrix, generated by our Monte Carlo program, representing the eigenspectrum of D is shown. The red dots, with a negative real part and a small imaginary part ($\mathrm{Im}(z)<|0.05|$ is a convenient choice for the illustration), represent the wanted eigenvalues. In figure 5.2 the eigenspectrum of the even-odd preconditioned matrix is shown. The red dots

correspond to the red dots in figure 5.1. Figures 5.3 and 5.4 show the eigenspectrum of the even-odd preconditioned matrix transformed by a power polynomial and by a Faber polynomial, respectively, which are the two polynomials presented in this thesis. The wanted eigenvalues (red dots) have now a larger real part in case of power polynomial and a larger magnitude in case of Faber polynomial. Therefore, if an iterative eigensolver is used on the even-odd preconditioned matrix, the eigenvectors corresponding to these eigenvalues are obtained first. The eigenvalues of the original matrix are then recovered using (4.17).

5.1. Power Polynomials

The implicit restart mechanism of ARPACK [17] allows one to calculate eigenvalues in an order with respect to one of the following criteria: largest magnitude (LM), smallest magnitude (SM), largest real part (LR), smallest real part (SR). The possibility to first calculate eigenvalues with largest real part was already exploited to obtain negative real eigenvalues of D in an efficient way [21]. The method is to shift D by some $\sigma \in \mathbb{R}$ and to exponentiate the results by $n \in \mathbb{N}$, that is,

$$P(\mathrm{D}) = (\mathrm{D} - \sigma)^n \tag{5.3}$$

so that the angle of each (not yet calculated) eigenvalue of $\hat{\mathrm{D}}$ with respect to σ, that is, $\theta_\sigma = \tan^{-1}(y/x_\sigma)$, is multiplied by n and the distance with respect to σ, that is, $r_\sigma = (y^2 + x_\sigma^2)^{1/2}$ is raised to the nth power, with $x_\sigma = x - \sigma$. In other words, each eigenvalue is rotated from θ_σ onto $n\theta_\sigma$ on an circle of radius nr_σ centered at σ. The coefficients of such a polynomial can be obtained by the binomial theorem

$$(z - \sigma)^n = \sum_{k=0}^{n} B_k \, (-\sigma)^{n-k} \, z^k \quad , \quad B_k \equiv \binom{n}{k} \equiv \frac{n!}{k!(n-k)!} \; . \tag{5.4}$$

An improved version of this method is to successively apply such polynomials on D. An iteration of, for instance, 4 steps would yield a polynomial of the form

$$P(\mathrm{D}) = ((((\mathrm{D} - \sigma_1)^{n_1} - \sigma_2)^{n_2} - \sigma_3)^{n_3} - \sigma_4)^{n_4} \; . \tag{5.5}$$

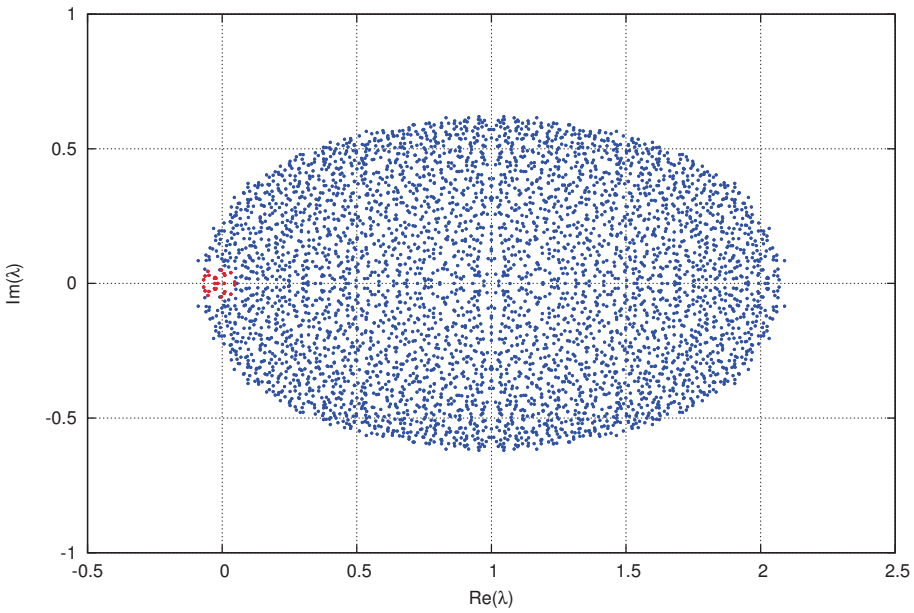

Figure 5.1.: Eigenspectrum of a random matrix representing the eigenspectrum of D. Red dots represent the wanted eigenvalues with Re(z)<0 and Im(z)<|0.05|.

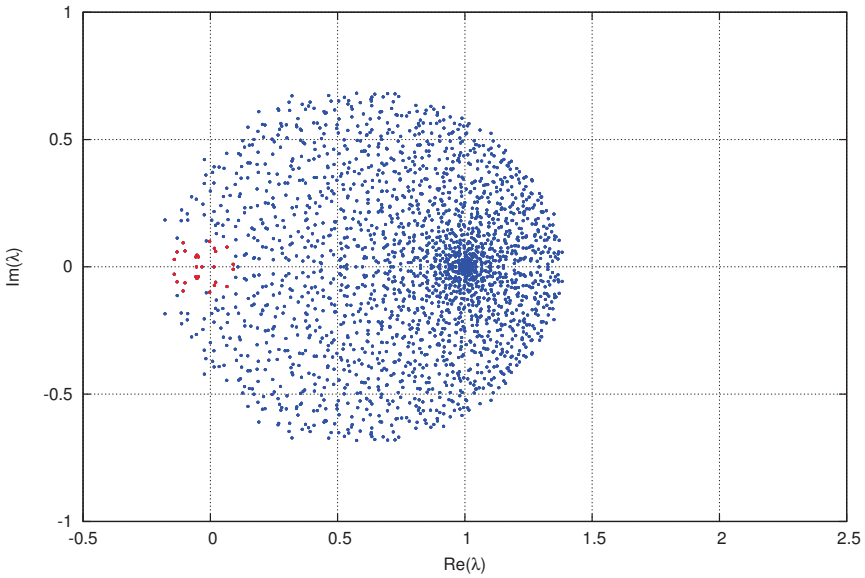

Figure 5.2.: Eigenspectrum of the even-odd preconditioned matrix, with the red dots representing the wanted eigenvalues

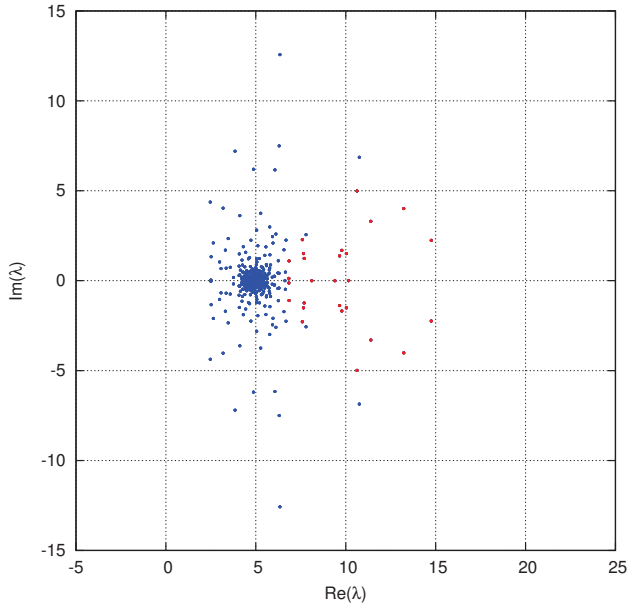

Figure 5.3.: Eigenspectrum of the even-odd preconditioned matrix transformed by a power polynomial, with the red dots representing the wanted eigenvalues, whose real part is amplified

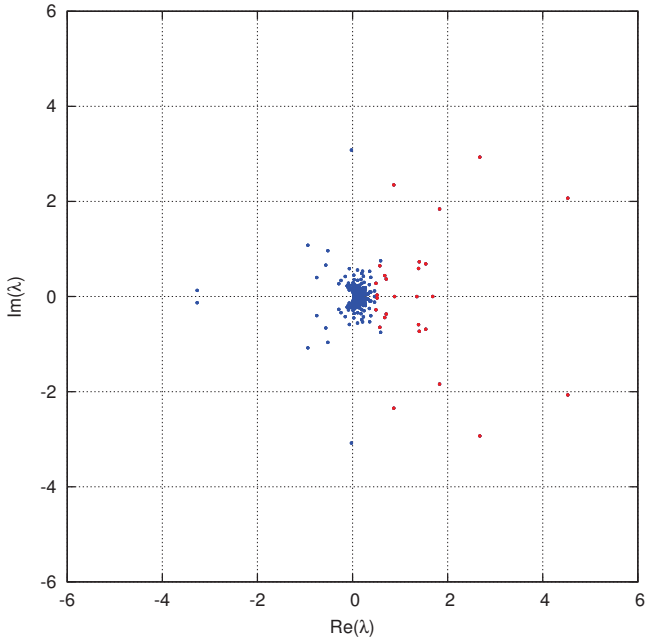

Figure 5.4.: Eigenspectrum of the even-odd preconditioned matrix transformed by a Faber polynomial, with the red dots representing the wanted eigenvalues, whose magnitude is amplified

5.1.1. Numerical Experiments

We tested 4 power polynomials of order 8, 16, 48 and 80, on the even-odd preconditioned Dirac-Wilson operator $\hat{\mathrm{D}}$ corresponding to configurations on the lattice of volume $32^3 \times 64$ with $\beta = 1.75$ and $\kappa = 0.1495$, which we used in numerical simulations of $\mathcal{N}$=1 SYM. The value of κ is large enough to observe negative real eigenvalues.

This method works if $\hat{\mathrm{D}}$ is flipped around the imaginary axis and the origin is shifted to -2 (or a smaller number), in other words, if $-\hat{\mathrm{D}} + 2$ is used as the matrix whose eigenvalues are to be calculated. In this way, it is ensured the smallest eigenvalues remain smallest when a power polynomial of even order is applied (figure 5.5).

This method has been extensively studied and technical details of choosing the correct parameters are discussed in [22] and [23]. Therefore we only present here the tests results, which are tabulated in table 5.1. The behavior of the real part of the power polynomial of order 8 is shown in figure 5.6. The peak means, keeping in mind that $\hat{\mathrm{D}}$ is flipped and shifted, that the eigenvalues near the origin are calculated first, because the eigenvectors corresponding to them have the largest real part after the transformation of $\hat{\mathrm{D}}$.

10 eigenvalues were calculated using these polynomials. The result obtained by using the power polynomial of order 8 is shown in figure 5.7. The grey points are the first 20 eigenvalues with the smallest real part, extracted by ARPACK in LR mode.

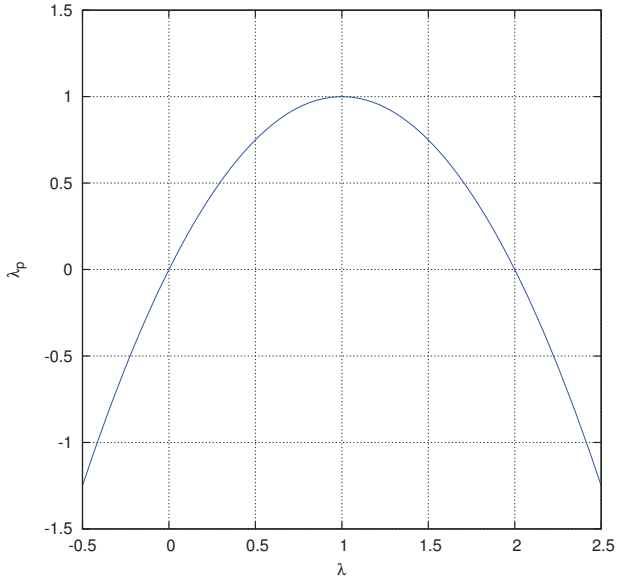

Figure 5.5.: Even-odd preconditioning of real eigenvalues

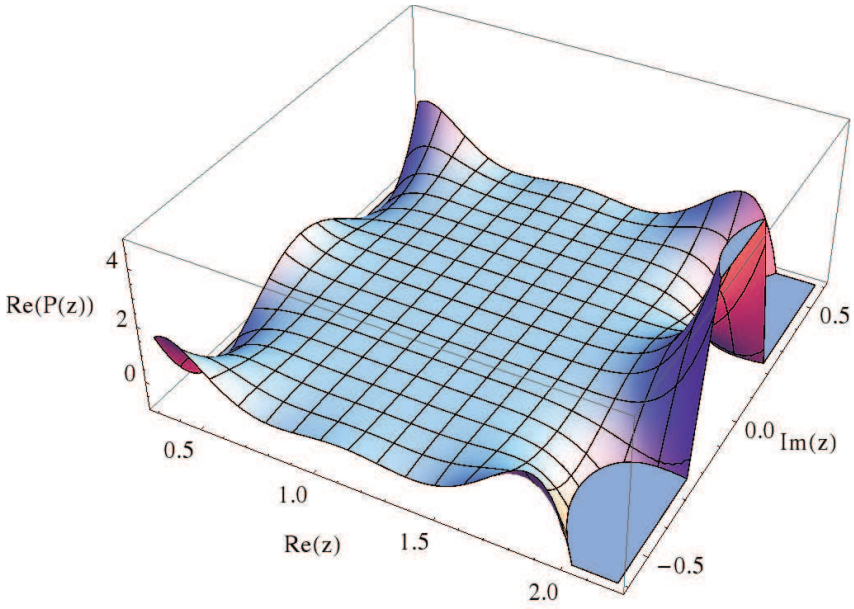

Figure 5.6.: Real part of a power polynomial of order 8

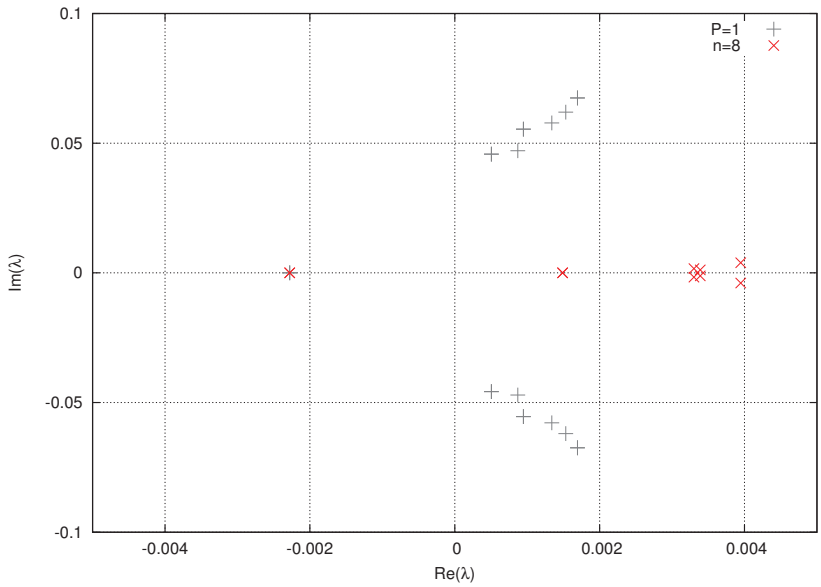

Figure 5.7.: Lowest 10 eigenvalues of D on the lattice of volume $32^3 \times 64$ with $\beta = 1.75$ and $\kappa = 0.1495$ calculated using the polynomial in the figure. Grey points are 20 eigenvalues calculated by ARPACK in LR mode.

5.2. Faber Polynomials

Faber polynomials [24] provide a basis for a convergent expansion of any function $f(z)$ continuous at every point and analytic at every interior point of G, which is a region in the complex plane bounded by a closed curve Γ and whose complement $\bar{G}$ is simply connected in the extended complex plane, that is, in $\hat{\mathbb{C}} \equiv \mathbb{C} \cup \{\infty\}$. Simply connected means any path connecting two points in the region can be deformed into another path without leaving the region. $f(z)$ can then be expressed as

$$f(z) = \sum_{n=0}^{\infty} a_n F_n(z) \ , \tag{5.6}$$

where F_n is the nth Faber polynomial corresponding to G. If $f(z)$ is also analytic on Γ, then the coefficients a_n are defined by

$$a_n = \frac{1}{2\pi \mathrm{i}} \int_{|w|=R} \frac{f(\Psi(w))}{w^{n+1}} dw \ , \tag{5.7}$$

where $\Psi(w)$ is the conformal (analytic, one-to-one and with a non-zero derivative everywhere) mapping which maps the complement of a closed disk E of radius ρ, denoted by $\bar{E}$, onto $\bar{G}$. R is the radius of the circle in $\bar{E}$ whose image under Ψ defines the level curve Γ_R, which is a Jordan curve, that is, a closed curve not self-crossing. Γ_R bounds the region I_R, to which f can be analytically extended. If Γ is already a Jordan curve, then R can be set to ρ. If f is not analytic on Γ, then the definition of a_n has $R = \rho$ if the integral exists [25].

The existence of $\Psi(w)$ and its inverse $\Phi(z)$, that is, the conformal mapping from $\bar{G}$ onto $\bar{E}$, is ensured by the Riemann's mapping theorem, which states that any simply connected region in the complex plane can be mapped conformally and one-to-one to any other such region except the entire plane.

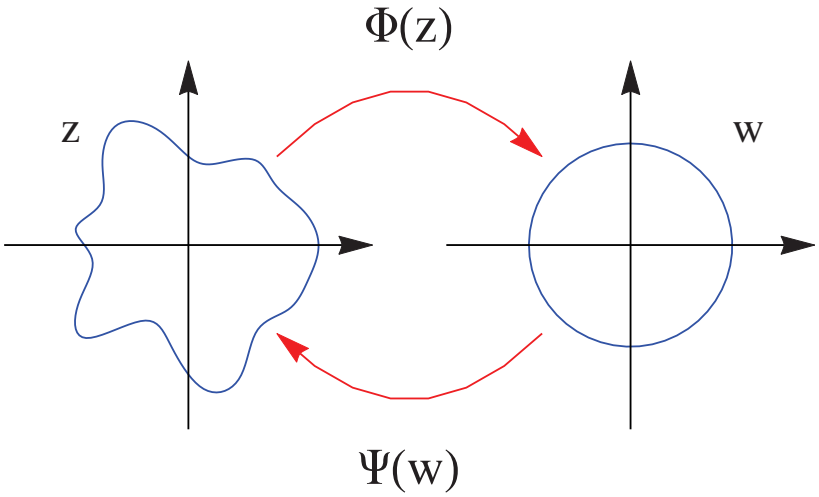

Figure 5.8.: Illustration of the exterior comformal mappings Φ and Ψ

One way to obtain F_n corresponding to G is to use the Laurent expansion of Φ in the neighborhood of its pole, which is ∞ :

$$\Phi(z) = \frac{z}{t} + d_0 + \frac{d_1}{z} + \frac{d_2}{z^2} + \dots \tag{5.8}$$

F_n is the polynomial part of $[\Phi(z)]^n$, that is, if

$$[\Phi(z)]^n = \sum_{k=-\infty}^{n} d_{nk}\, z^k \tag{5.9}$$

then

$$[\Phi(z)]^n \equiv \sum_{k=-\infty}^{-1} d_{nk}\, z^k + F_n(z) \ . \tag{5.10}$$

If Ψ is known, Faber polynomials can also be computed recursively using the Laurent expansion coefficients of its inverse map

$$\Psi(w) = t\left[w + c_0 + \frac{c_1}{w} + \frac{c_2}{w^2} + \dots\right] \quad , \quad t > 0 \tag{5.11}$$

as

$$\begin{aligned} F_0 = 1 \ , \quad F_1 = z/t - c_0 \ , \\ F_{n+1} = F_1 F_n - \sum_{k=1}^{n} c_k F_{n-k} - n c_n \ . \end{aligned} \tag{5.12}$$

These polynomials were studied in the framework of polynomial iterative methods used for solving linear systems of equations $Ax = b$ [26–28]. The system is solved by iterating an initial vector x_0 by $x_n = x_0 + q_{n-1}(A)r_0$ to minimize the residual $r_n = b - Ax_n = (1 - Aq_{n-1}(a))r_0 = p_n(A)r_0$. Since

$$r_n = p_n(A)r_0 = p_n(A)\sum_{i=1}^{N} a_i v_i = \sum_{i=1}^{N} p_n(\lambda_i)\, a_i v_i \ , \tag{5.13}$$

where v_i are the eigenvectors of A and, for any norm,

$$||r_n|| \le ||p_n(A)||\, ||r_0|| \ , \tag{5.14}$$

one should use a p_n such that

$$||p_n|| \le ||p|| \ , \quad \text{for all} \quad p \in P_n \ , \tag{5.15}$$

where

$$||p|| \equiv \max_{z \in G} |p(z)| \tag{5.16}$$

denotes the uniform norm in G, the region containing the eigenvalues of A. $P(0) = 1$ by definition and the convergence of the iteration requires $0 \notin G$. This latter is a convenient condition for us because we are interested in negative real eigenvalues.

It was proven that under certain assumptions concerning G, normalized Faber polynomials

$$\tilde{F}_n(z) \equiv \frac{F_n(z)}{F_n(0)}, \quad n \geq 0 \tag{5.17}$$

are nearly exact solutions to (5.15) as $n \to \infty$ if G is convex and optimal enough for practical purposes if G is non-convex [27].

Exterior conformal maps Φ and Ψ, from which corresponding Faber polynomials are constructed, are only known explicitly for certain types of regions, such as square, rectangle, semi-disk [29], circular arc [30], circular disks [31], elliptic disks, annular regions [32], arbitrary circular disk and bratwurst-shaped regions [28]. For other types of regions, such as polygons, numerical conformal mapping should be used [33, 34].

We consider only non-convex polygons and bratwurst-shaped regions, since these are the ones that can contain uninteresting eigenvalues of D.

5.2.1. Schwarz-Christoffel Mapping

Schwarz-Christoffel mapping f is a conformal mapping from some region D to G, where G is bounded by a polygon with vertices $v_n = f(u_n)$ and interior angles $\alpha_n\pi$ in counterclockwise order. If D is the unit disk E and $\bar{G}$ the exterior polygon with angles $(1-\alpha_n)\pi$, then

$$f(u) = A + C\int^u \zeta^{-2} \prod_{k=1}^{n} \left(1 - \frac{\zeta}{u_k}\right)^{1-\alpha_k} d\zeta \ , \tag{5.18}$$

for some complex constants A and C [33]. An exterior mapping $\Phi(z)$ from $\bar{G}$ to $\bar{E}$ and its inverse $\Psi(w)$ exist because both regions are simply connected. Then $\Psi(w) = f(1/w)$. Figure 5.9 illustrates all three mappings f, Φ and Ψ and their relations. The coefficients of its Laurent expansion, which are used to recursively construct corresponding Faber polynomials, have a non-trivial form and listed in [27].

5.2.2. Conformal Bratwurst Mapping

For G with an analytic and non-convex boundary, there is a conformal mapping from $\bar{E}$ to $\bar{G}$ of the form

$$\Psi = \psi_2 \circ J \circ \psi_1 \tag{5.19}$$

where ψ_2 and ψ_1 are certain Möbius transformations and J certain Joukowsky transformation. The first Möbius transformation is (figure 5.10*b*)

$$\psi_1 = (1+\epsilon)\frac{\mathrm{i}P_\infty z + \lambda_m(1+\epsilon)}{\mathrm{i}(1+\epsilon)z + \lambda_m P_\infty^*}, \ \ \epsilon \in [0, \epsilon_{max}) \ , \tag{5.20}$$

where

$$\epsilon_{max} := \tan\frac{\phi}{4}\left(1 + \tan\frac{\phi}{8}\right)$$

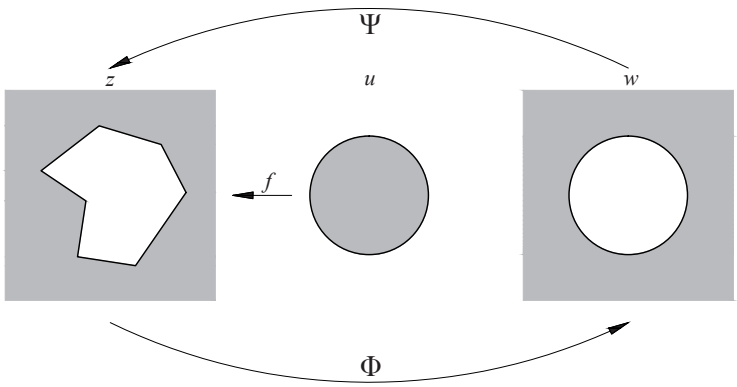

Figure 5.9.: Illustration of the mappings f, Φ and Ψ

and

$$P_\infty = \mathrm{i}\left(\tan\frac{\phi}{4} + \left(\cos\frac{\phi}{4}\right)^{-1}\right), \quad \phi \in (0, 2\pi). \tag{5.21}$$

It maps the exterior of the unit circle onto the exterior of a bigger circle with its center on the origin and with a diameter of $1+\epsilon$ (figure 5.10b). The exterior of this circle is then mapped onto the exterior of an ellipse by the Joukowsky transformation (figure 5.10c)

$$J(z) = \frac{1}{2}\left(z + \frac{1}{z}\right). \tag{5.22}$$

Finally, the real axis is mapped onto the unit circle by another Möbius transformation (figure 5.10d),

$$\psi_2 = \lambda_m \frac{z + i\tan\frac{\phi}{4}}{z - i\tan\frac{\phi}{4}}. \tag{5.23}$$

The complete conformal mapping then is

$$\Psi(z) = \lambda_m \frac{\psi_1^2(z) + 2\mathrm{i}\tan\frac{\phi}{4}\psi_1(z) + 1}{\psi_1^2(z) - 2\mathrm{i}\tan\frac{\phi}{4}\psi_1(z) + 1}, \tag{5.24}$$

which can be rewritten as

$$\Psi(z) = \frac{(z - \lambda_m N_\epsilon)(z - \lambda_m M_\epsilon)}{(N_\epsilon - M_\epsilon)z + \lambda_m(N_\epsilon M_\epsilon - 1)} \tag{5.25}$$

with

$$N_\epsilon = \frac{1}{2}\left(\frac{|P_\infty|}{1+\epsilon} + \frac{1+\epsilon}{|P_\infty|}\right), \quad M_\epsilon = \frac{(1+\epsilon)^2 - 1}{2\tan\frac{\phi}{4}(1+\epsilon)}. \tag{5.26}$$

The map depends on three parameters only, namely ϵ, ϕ und λ_m. λ_m is the orientation of the inclusion set, ϵ changes its thickness along the real axis and ϕ is the angle of the opening of the non-convex curve of the boundary of the inclusion set with respect to origin.

The coefficients of its Laurent expansion are

$$c_0 = -\lambda_m(N_\epsilon + M_\epsilon + S_\epsilon), \tag{5.27}$$

$$c_n = (\lambda_m S_\epsilon)^{n-1}\lambda_m^2(S_\epsilon - N_\epsilon)(S_\epsilon - M_\epsilon),\ n \geq 1 \tag{5.28}$$

where

$$S_\epsilon := \frac{N_\epsilon M_\epsilon - 1}{N_\epsilon - M_\epsilon} \quad , \quad t = \frac{s}{N_\epsilon - M_\epsilon}\ , \tag{5.29}$$

with s is a positive real number which scales the elements of the inclusion set.

5.2.3. Numerical Experiments

The Faber polynomials corresponding to regions defined by Schwarz-Christoffel (SC) and Bratwurst (BW) mappings were tested on the even-odd preconditioned Dirac-Wilson operator $\hat{\mathrm{D}}$ corresponding to configurations on the lattice of volume $32^3 \times 64$ with $\beta = 1.75$ and $\kappa = 0.1495$, which we used in numerical simulations of $\mathcal{N}$=1 SYM. The value of κ is large enough to observe negative real eigenvalues.

For illustration purposes, the lattice of volume $6^3 \times 8$ with $\beta = 1.6$ and $\kappa = 0.1599$ was used. It is the largest volumes, which we could diagonalize completely, and its κ is large enough for observing eigenvalues in the left half-plane.

We used a package for numerical conformal mapping named the Schwarz-Christoffel Toolbox [35,36] written in MATLAB for SC mappings and a script that we have written in Mathematica for BW mappings.

First, the extremal eigenvalues of $\hat{\mathrm{D}}$ for one configuration were obtained using ARPACK. Then curves to enclose uninteresting eigenvalues were designed. The procedure is illustrated in figures 5.10, 5.12 and 5.20. The purple ellipse in figures 5.10 and 5.12 represent the eigenspectrum of $\hat{\mathrm{D}}$ and the blue curve the boundary of the region for the BW mapping used for generating the corresponding Faber polynomials. In figure 5.20, the eigenspectrum of $\hat{\mathrm{D}}$ on the smaller lattice is shown with the polygon enclosing the uninteresting eigenvalues. The curves outside the polygon are preimages of circles of radius R outside the unit disk, that is, they visualize Ψ.

Faber polynomials of different orders were tested in order to examine the effect of the order of the polynomial on the optimality, in the sense of (5.15), and on the duration of the eigenvalue extraction. The results concerning the optimality are shown in figures 5.14-5.17 and 5.22-5.25. The magnitude of the Faber polynomials of different order in the region where the eigenspectrum of $\hat{\mathrm{D}}$ is located are plotted against the complex plain as a mesh. The polyonomials in the first four pictures were generated using the MW mapping, and the second four using the SC mapping. The peak seen near the origin is the transformation that we want, as illustrated in figures 5.1 and 5.4. It implies that the eigenvectors corresponding to the eigenvalues near the origin will have larger

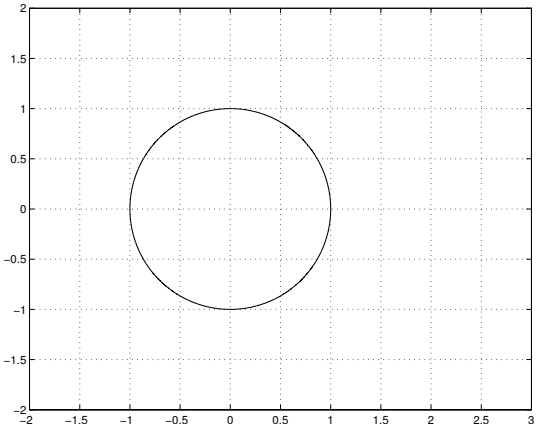

(a) Unit circle

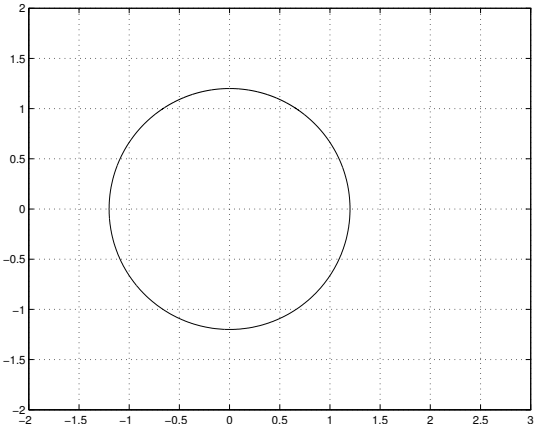

(b) Boundary of the inclusion set after the first Möbius transformation with $\epsilon = 0.2$, $\phi = \pi/2$, $\lambda_m = -1$

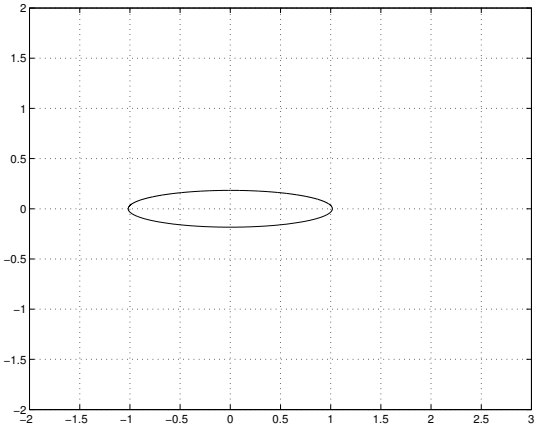

(c) Boundary of the inclusion set after the Joukowsky transformation

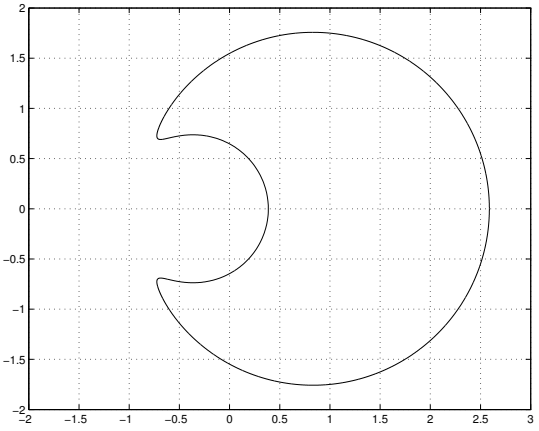

(d) Boundary of the inclusion set after the second Möbius transformation

eigenvalues after a Faber polynomial is applied on $\hat{\mathrm{D}}$. The eigenvalues in the left half-plane are amplified more drastically.

The boundary of the curve is approximated more and more by increasing the order, as expected from its definition (5.9). But, there is a limit to the order due to numerical instabilities, as seen in figures 5.16 and 5.25. As the order increases, numerical instabilities emerges, limiting the order to around 30 for SC mappings and 40 for BW mappings. This limitation lead us to test Faber polynomials shifted by some real σ, $F(z-\sigma)$, since the derivative of the polynomial is much higher outside the boundary. The mesh plot of a 40th Faber polynomial shifted by $\sigma = 0.2$ is shown in figure 5.17. There is also a lower limit to the order, in the sense that the expected behavior is not observed, as seen in figure 5.22.

The figures 5.11, 5.13 and 5.21 are only meant to illustrate how the application of a polynomial determines which eigenvalues are calculated. The complete eigenspectrum of $\hat{\mathrm{D}}$ on the smaller lattice is shown in gray points. The red points are the first 500 eigenvalues calculated first after a Faber polynomial is applied on $\hat{\mathrm{D}}$.

The tests on the configurations with negative real eigenvalues on the larger lattice were done for 10 eigenvalues. Testing on a higher number of eigenvalues would mean to enter the region bounded by the curve, where eigenvalue density becomes very high after the mapping. The polynomials illustrated by the mesh plots and their shifted forms were tested. The results are shown in figures 5.18, 5.19 and 5.26 and tabulated in table 5.1. The results concerning the power polynomials tested are also listed in the table for comparison.

In the table are listed the tested polynomials, the total number of matrix-vector multiplications executed by ARPACK, the time spent for matrix-vector multiplications needed by ARPACK for applying $P(\hat{\mathrm{D}})$ on the iterated vector and the total executation time for calculating 10 eigenvalues. The polynomials are symbolized in the following way. P means power polynomial, except $P = 1$, which means no polynomials were used. F stand for Faber polynomial. Its superscript is either a number, which is the ϵ of the corresponding BW mapping, or SC, which implies the polygon in figure 5.20. The subscript is the order of the polynomial for both P and F. $\phi = \pi/2$ for the BW mappings.

The grey points in the figures are the first 20 eigenvalues with the smallest real part, which are extracted by ARPACK in LR mode. They are included in the figure for comparison. The red and blue points in the first two figures are 10 eigenvalues of $\hat{\mathrm{D}}$ obtained using the 40th Faber polynomial corresponding to the BW mapping with $\epsilon = 0.3$ and $\epsilon = 0.22$, respectively and their shifted form with $\sigma = 0.2$. We can see that in case of $\epsilon = 0.3$ the shifted polynomial magnifies eigenvalues closer to the real axis better, and as seen in the table 5.1, its yields much faster eigenvalue extraction. In case of $\epsilon = 0.22$, the non-shifted polynomial yielded only 0's. In third figure, we see a comparison of the results obtained using the 20th, 30th and 40th Faber polynomials corresponding to the SC mapping in figure 5.20. The second polynomial magnifies eigenvalues closer to the real axis better, but as seen in the table, the first one yields a faster eigenvalue extraction, therefore it may be preferable over the second one if there are only a few negative real eigenvalues, as is the case here.

The tabulated results shows that power polynomials, combined with the LR mode of ARPACK yields the highest acceleration, provided that the correct set of shift and power parameters are discovered. A power polynomial of order as high as 80 can yield a fast eigenvalue extraction in spite of the long duration needed for the matrix-vector calculation done in one Arnoldi iteration. On the other hand, a power polynomial with of a lower order like 16 can show a relatively low performance.

Faber polynomials in their original form do not provide an acceleration comparable to that of power polynomials, mainly due to numerical instabilities arising at higher orders, preventing us from increasing the optimality of Faber polynomials beyond some level. However, their shifted forms result in acceleration comparable to that of power polynomials. They are also not bound by the LR mode of ARPACK and further tests can be done by integrating them into restarting schemes of iterative eigensolvers.

Polynomial	$\#P(\hat{\mathrm{D}})v$	Time for $P(\hat{\mathrm{D}})v$ (s)	Time (s)
P_8(z)	1513	0.48	350.96
P_{80}(z)	281	2.03	505.73
$F_{40}^{0.3}$(z-0.2)	640	0.82	540.87
$F_{40}^{0.3}$(z-0.15)	733	0.82	622.35
P_{48}(z)	575	1.05	629.15
P_{16}(z)	1777	0.39	778.77
$F_{40}^{0.3}$(z-0.1)	974	0.93	821.47
$F_{40}^{0.22}$(z-0.2)	1012	0.9	852.02
F_{20}^{SC}(z)	1998	0.44	962.41
$F_{40}^{0.22}$(z-0.15)	1483	0.81	1241.6
F_{30}^{SC}(z)	2042	0.64	1403.2
$F_{40}^{0.22}$(z-0.1)	1708	0.82	1432.4
$F_{40}^{0.3}$(z)	1752	0.82	1526.4
$P = 1$	60120	0.07	7053.7

Table 5.1.: Results of the polynomial preconditioning tests. P means power polynomial, except $P = 1$, which means no polynomials were used. F stand for Faber polynomial. Its superscript is either a number, which is the ϵ of the corresponding BW mapping, or SC, which implies the polygon in figure 5.20. The subscript is the order of the polynomial for both P and F.$\phi = \pi/2$ for the BW mappings.

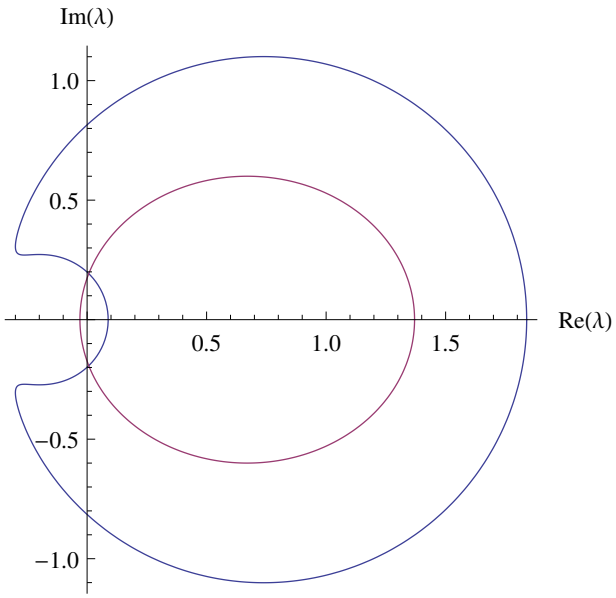

Figure 5.10.: Boundary of the BW mapping with $\epsilon = 0.3$ and $\phi = \pi/2$, scaled in accordance with the eigenspectrum represented by the purple ellipse

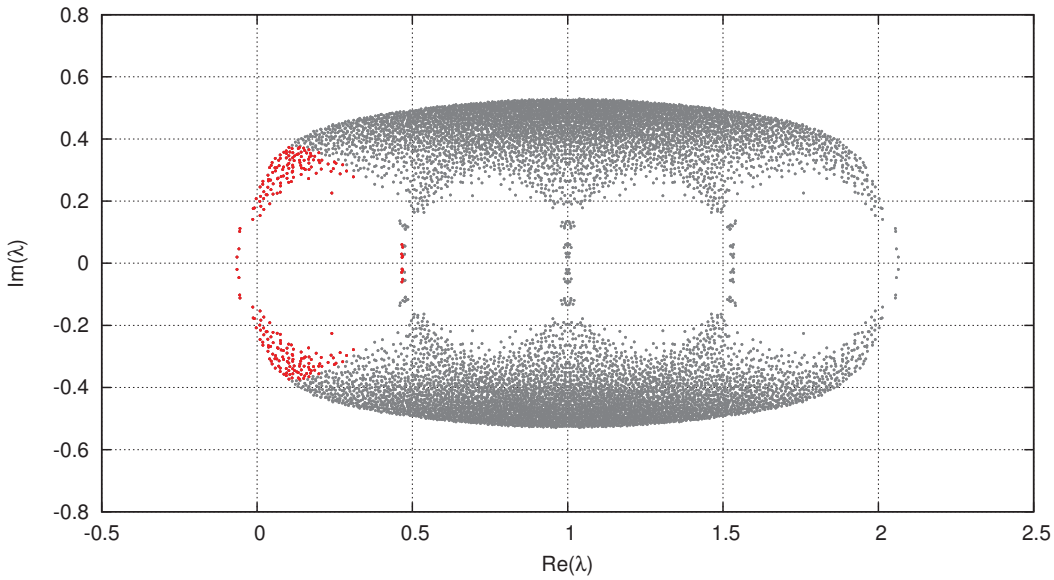

Figure 5.11.: Eigenvalues of D on a lattice of volume $6^3 \times 8$ ($\beta = 1.6$, $\kappa = 0.1599$) calculated using the 40th Faber polynomial corresponding to the BW mapping in the previous figure

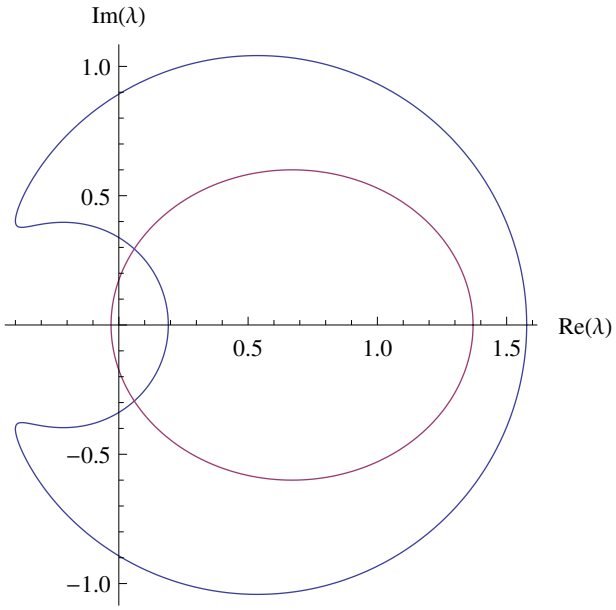

Figure 5.12.: Boundary of the BW mapping with $\epsilon = 0.22$ and $\phi = \pi/2$, scaled in accordance with the eigenspectrum represented by the purple ellipse

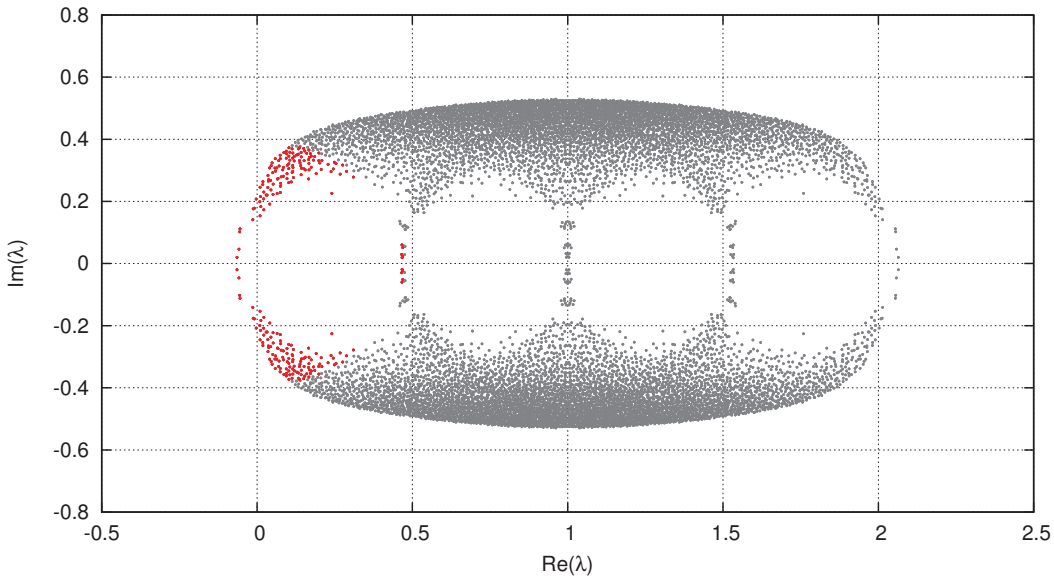

Figure 5.13.: Eigenvalues of D on a lattice of volume $6^3 \times 8$ ($\beta = 1.6$, $\kappa = 0.1599$) calculated using the 40th Faber polynomial corresponding to the BW mapping in the previous figure

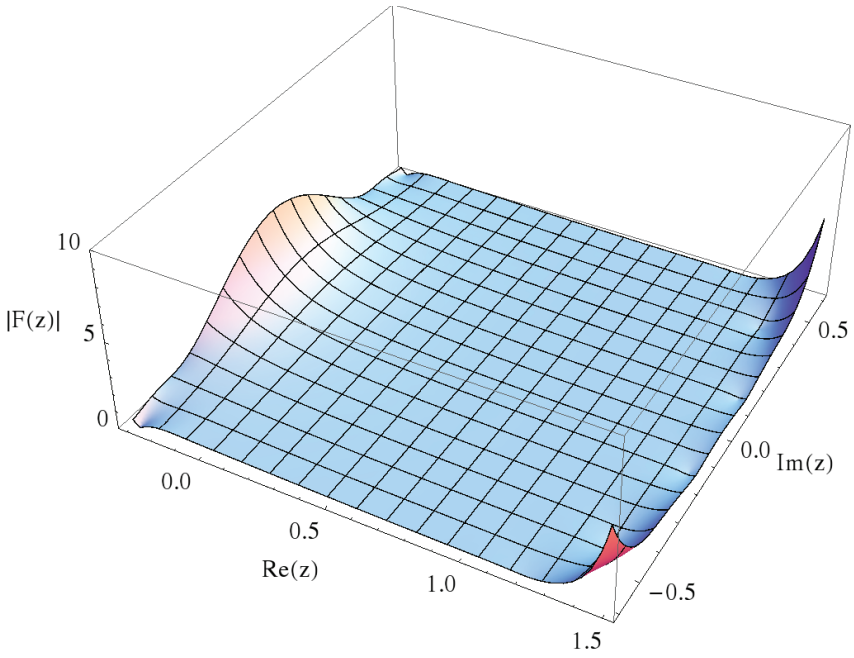

Figure 5.14.: Magnitude of the 20th Faber polynomial corresponding to the BW mapping illustrated in figure 5.12

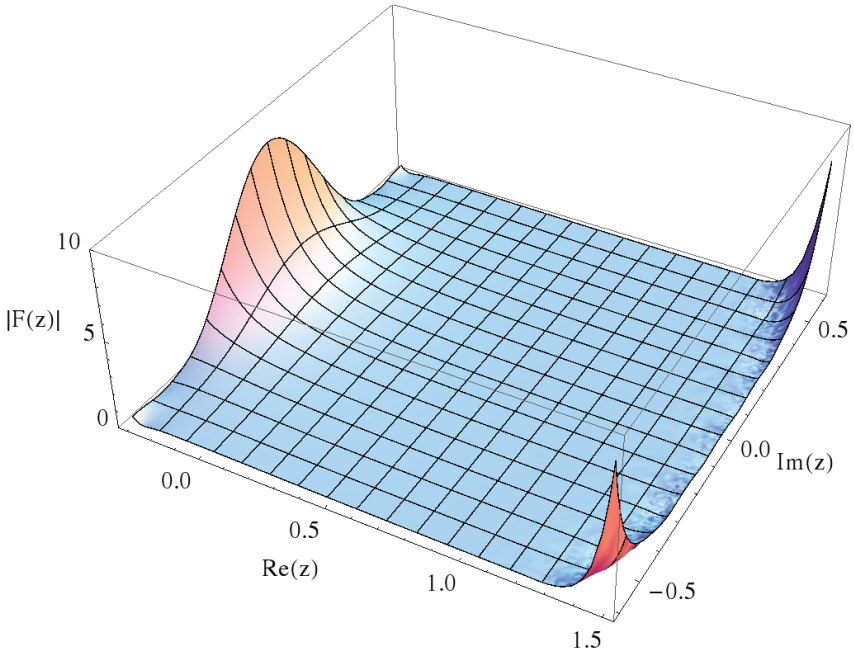

Figure 5.15.: Magnitude of the 30th Faber polynomial corresponding to the BW mapping illustrated in figure 5.12

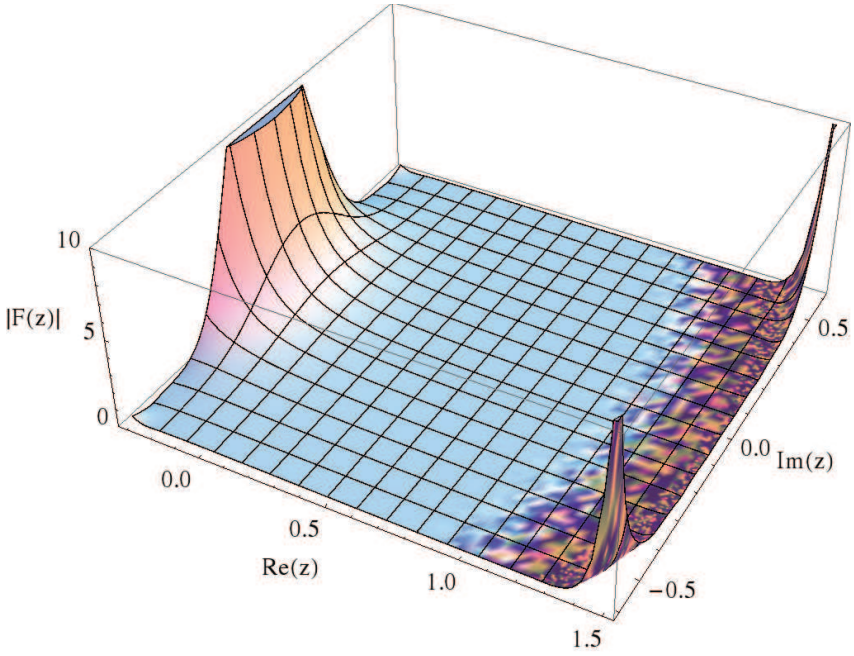

Figure 5.16.: Magnitude of the 40th Faber polynomial corresponding to the BW mapping illustrated in figure 5.12

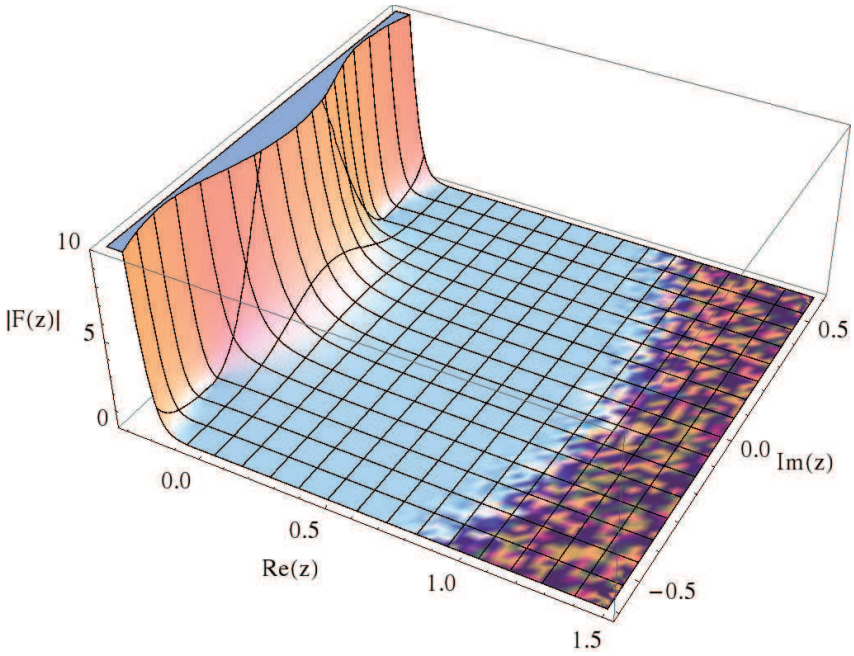

Figure 5.17.: Magnitude of the 40th Faber polynomial corresponding to the BW mapping illustrated in figure 5.12 shifted by 0.2

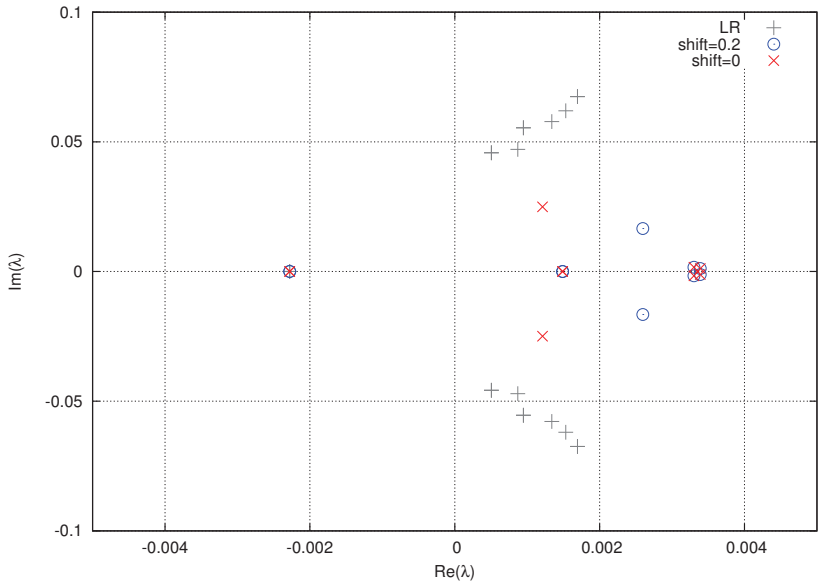

Figure 5.18.: Lowest 10 eigenvalues of D on the lattice of volume $32^3 \times 64$ with $\beta = 1.75$ and $\kappa = 0.1495$ calculated using $F_{40}^{0.3}(z)$ and $F_{40}^{0.3}(z-0.2)$. Grey points are 20 eigenvalues calculated by ARPACK in LR mode

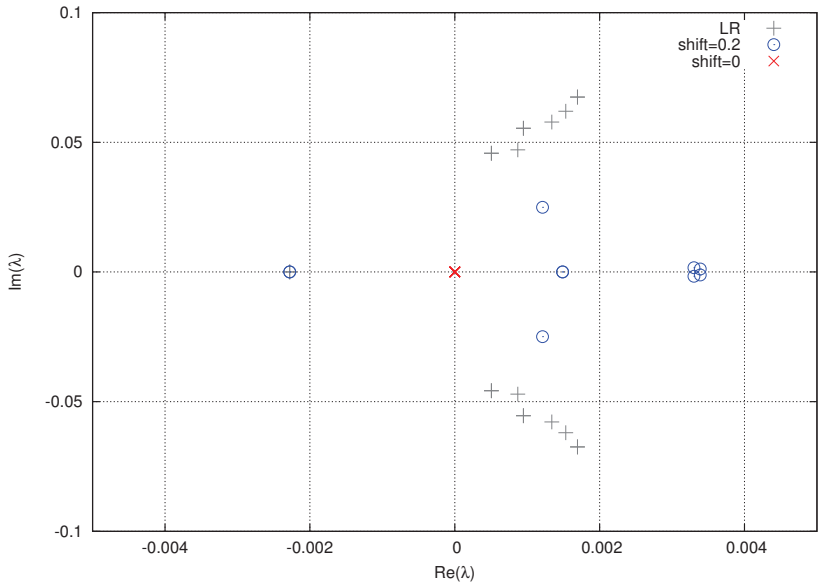

Figure 5.19.: Lowest 10 eigenvalues of D on the lattice of volume $32^3 \times 64$ with $\beta = 1.75$ and $\kappa = 0.1495$ calculated using $F_{40}^{0.22}(z)$ and $F_{40}^{0.22}(z-0.2)$. Grey points are 20 eigenvalues calculated by ARPACK in LR mode. The red cross means that no eigenvalues could be calculated using F_{40} due to numerical instabilities seen in Fig. 5.16.

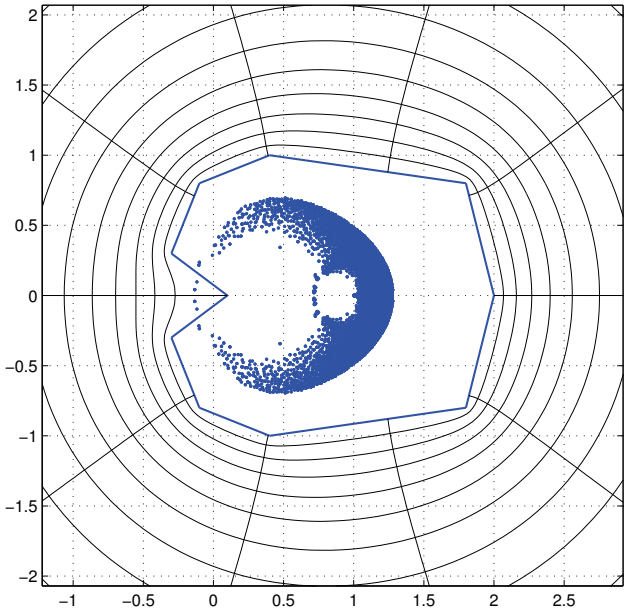

Figure 5.20.: A polygon enclosing the eigenspectrum of the mass-preconditioned D created using the SC Toolbox. The curves outside the polygon are preimages of circles of radius R outside the unit disk

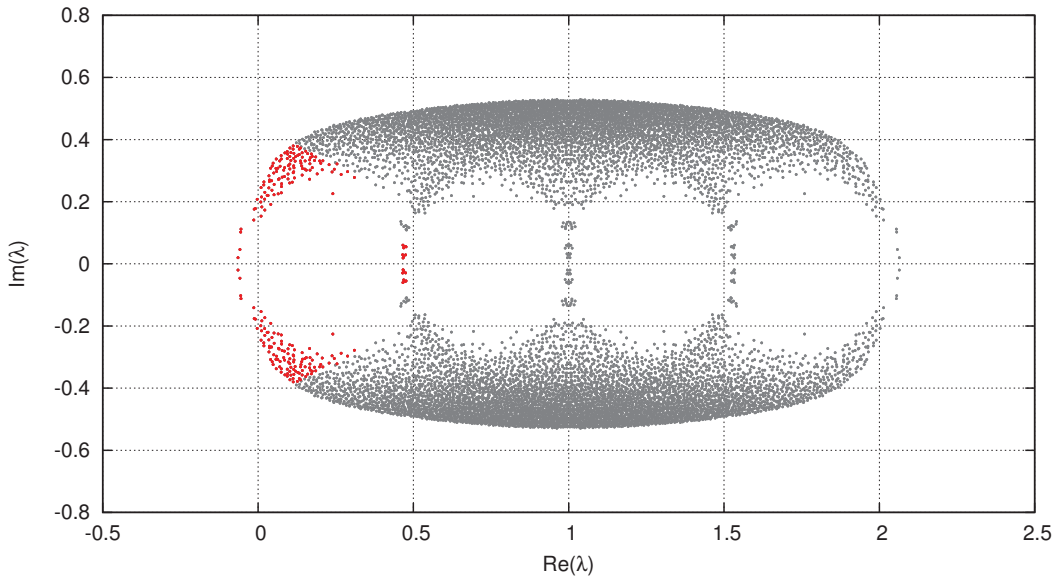

Figure 5.21.: Eigenvalues of D on a lattice of volume 6^3x8 ($\beta = 1.6$, $\kappa = 0.1599$) calculated using the 30th Faber polynomial corresponding to the SC mapping in the previous figure

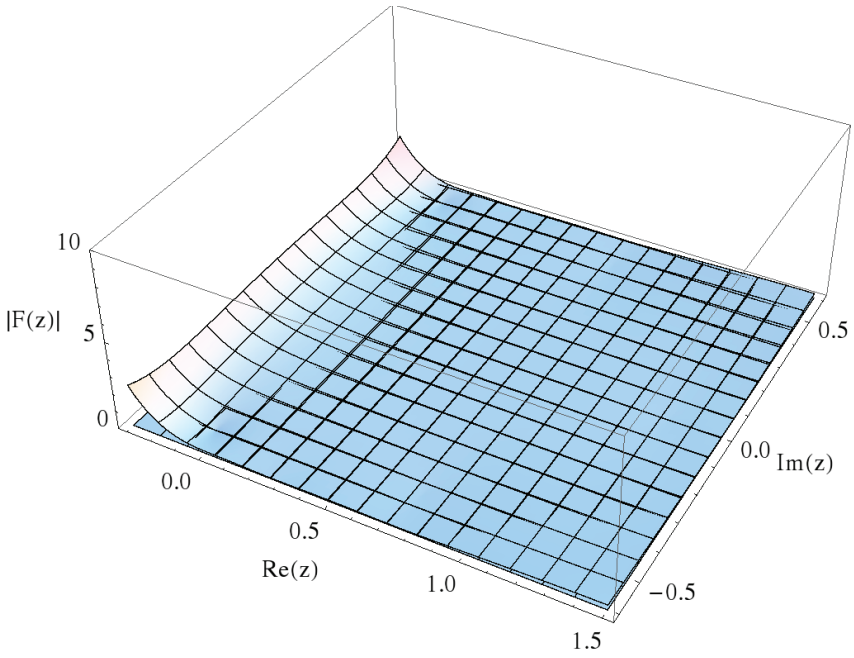

Figure 5.22.: Magnitude of the 10th Faber polynomial corresponding to the SC mapping illustrated in figure 5.20

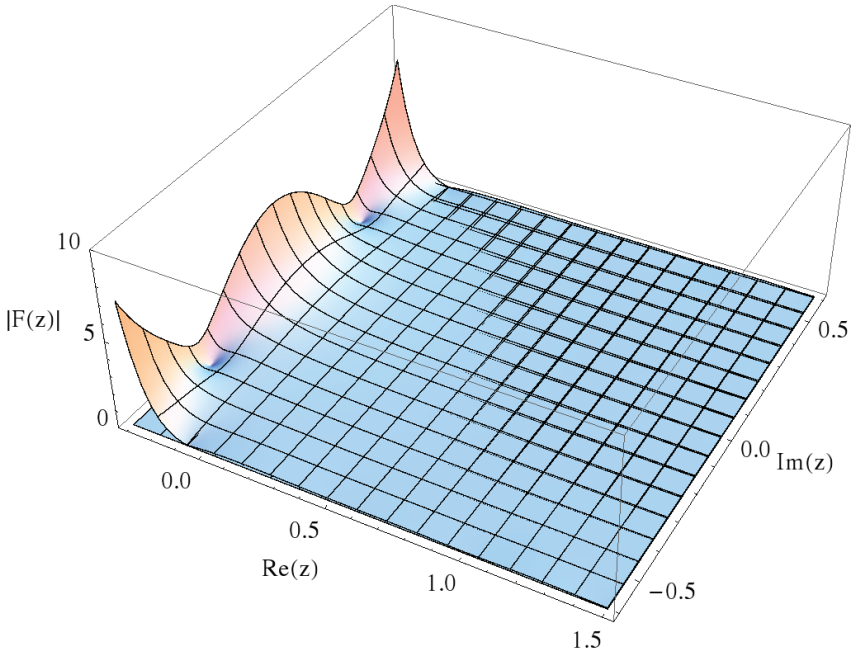

Figure 5.23.: Magnitude of the 20th Faber polynomial corresponding to the SC mapping illustrated in figure 5.20

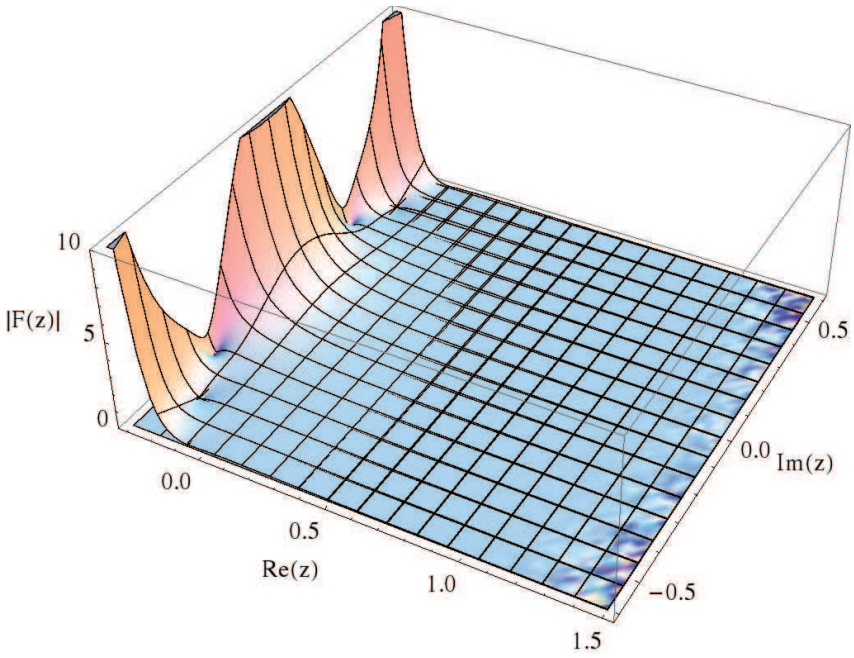

Figure 5.24.: Magnitude of the 30th Faber polynomial corresponding to the SC mapping illustrated in figure 5.20

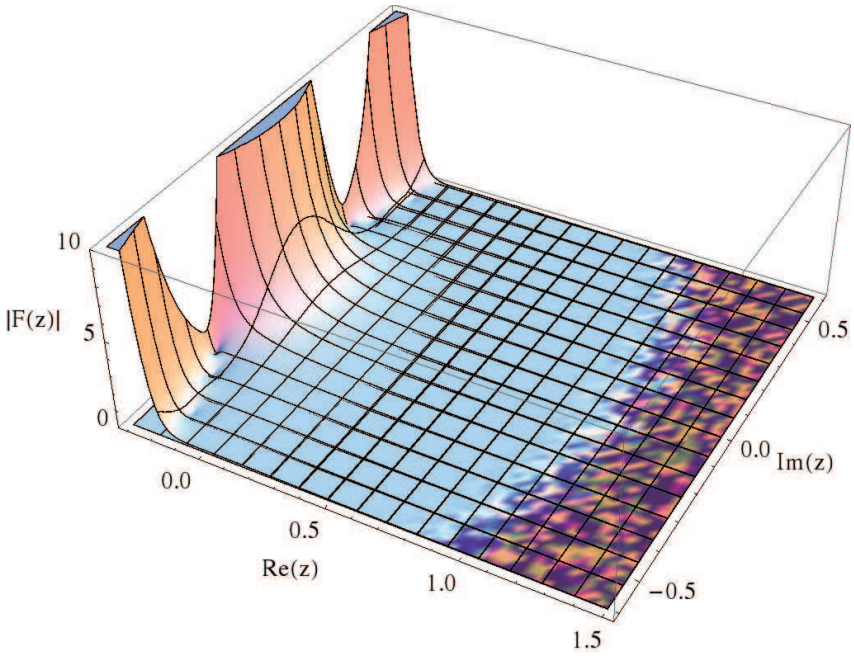

Figure 5.25.: Magnitude of the 40th Faber polynomial corresponding to the SC mapping illustrated in figure 5.20

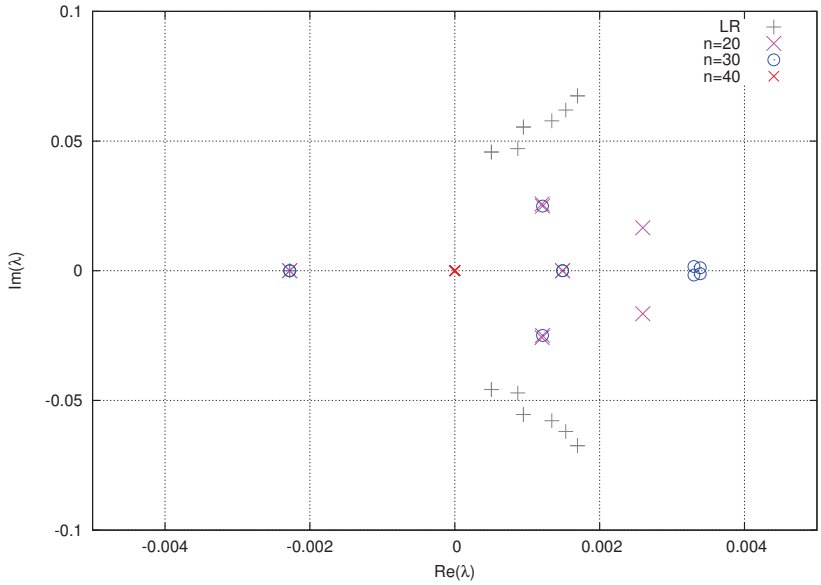

Figure 5.26.: Lowest 10 eigenvalues of D on the lattice of volume $32^3 \times 64$ with $\beta = 1.75$ and $\kappa = 0.1495$ calculated using $F_{20}^{SC}(z)$ and $F_{30}^{SC}(z)$. Grey points are 20 eigenvalues calculated by ARPACK in LR mode. The red cross means that no eigenvalues could be calculated using F_{40} due to numerical instabilities seen in figure 5.25.

6. Lattice simulations and results

The two low-energy mass supermultiplets of the bound states predicted by the effective theories in chapter 2 were confronted with numerical simulations on the lattice. We used data from lattices of dimension $24^3 \times 48$, $24^3 \times 64$ and $32^3 \times 64$ at β=1.75 and different κ values. We have chosen the spatial volume such that the effect of finite volume on supersymmetry breaking already induced by spacetime discretization and nonzero gluino mass were minimized. The masses were extracted from the two-point correlation functions of the lattice versions of the operators corresponding to the bound states, whose values decay exponentially with mass.

6.1. Correlators

6.1.1. Spin-1/2 Bound States

The gluino-glue particle is represented by the operator

$$O_{g\tilde{g}} = \sigma_{\mu\nu} F^a_{\mu\nu} \lambda^a \ , \tag{6.1}$$

where the Dirac indices are dropped as before. On the lattice, $F^a_{\mu\nu}$ is represented by the anti-Hermitian part of the clover plaquette $P^c_{\mu\nu}$,

$$U_{x,\mu\nu} = \frac{1}{8\mathrm{i}g_0}(P^c_{x,\mu\nu} - P^{c\,\dagger}_{x,\mu\nu}) \ , \tag{6.2}$$

to ensure that its properties under parity and time reversal transformations are preserved [37]. The clover plaquette $P^c_{\mu\nu}$ is formed of links in the fundamental representation:

$$\begin{aligned} P^c_{x,\mu\nu} = & U_{x\mu} U_{x+\hat{\mu},\nu} U^\dagger_{x+\hat{\nu},\mu} U^\dagger_{x\nu} + U^\dagger_{x-\hat{\nu},\nu} U_{x-\hat{\nu},\mu} U_{x-\hat{\nu}+\hat{\mu},\nu} U^\dagger_{x\mu} \\ & + U^\dagger_{x-\hat{\mu},\mu} U^\dagger_{x-\hat{\mu}-\hat{\nu},\mu} U_{x-\hat{\nu}-\hat{\mu},\mu} U_{x-\nu,\nu} + U_{x\nu} U^\dagger_{x-\hat{\mu}+\hat{\nu},\mu} U^\dagger_{x-\hat{\mu},\nu} U_{x-\hat{\mu},\mu} \ . \end{aligned} \tag{6.3}$$

The corresponding lattice operator then is after dropping the spacetime index x,

$$O_{g\tilde{g}} = \sum_{i<j} \sigma_{ij} \,\mathrm{tr}\, U_{ij} \lambda \tag{6.4}$$

where trace is over color indices and i and j are only the spatial directions.

The corresponding correlator is

$$C_{g\tilde{g}}(x_0 - y_0) = -\frac{1}{4} \langle \sigma^{\alpha\beta}_{ij} \,\mathrm{tr}\,[U_{x,ij} T^a] (\mathrm{D}^{-1})^{ab,\beta\rho}_{xy} \ , \mathrm{tr}\,[U_{y,kl} T^b] \sigma^{\alpha\rho}_{kl} \rangle \tag{6.5}$$

where repeated indices imply summation. At large distances the correlator takes the form

$$C_{g\tilde{g}} \simeq C \sinh(m\,(t - T/2)) \;, \tag{6.6}$$

where T is the temporal extent of the lattice. The mass m of the gluino-glue then is obtained by fitting this function to the correlator (6.5).

6.1.2. Adjoint Mesons

The two mesons belonging to the same multiplet, namely the scalar adjoint meson $a - f_0$ and the pseudoscalar adjoint meson $a - \eta'$ are represented in respective order by

$$O_{a-f_0} = \bar{\lambda}\lambda \quad , \quad O_{a-\eta'} = \bar{\lambda}\gamma_5\lambda \tag{6.7}$$

The corresponding correlators consisting of connected and disconnected pieces are, with $\Gamma = 1$ for $a - f_0$ and $\Gamma = \gamma_5$ for $a - \eta'$,

$$\begin{aligned} C(x_0 - y_0) &= C_c(x_0 - y_0) + C_d(x_0 - y_0) \\ &= \frac{1}{L^3}\langle \mathrm{tr}\,[\Gamma\, \mathrm{D}^{-1}_{xy}\, \Gamma\, \mathrm{D}^{-1}_{yx}]\rangle - \frac{1}{2L^3}\langle \mathrm{tr}\,[\Gamma\, \mathrm{D}^{-1}_{xx}]\,\mathrm{tr}\,[\Gamma\, \mathrm{D}^{-1}_{yy}]\rangle \;, \end{aligned} \tag{6.8}$$

where terms are summed over repeated indices. C_d was calculated using the stochastic estimator method [38].

6.1.3. 0^+ and 0^- Glueballs

The scalar and pseudoscalar glueballs belonging to the other multiplet are given by a linear combination of several closed linked loops. The loops representing the scalar glueball can be rotated into their mirror image while the ones representing the pseudoscalar glueball cannot as their names suggest.

6.2. Finite-Size Effects

We investigated [39] the effect of the finite volume of the lattice on the masses by extrapolating the masses of the fermionic gluino-glue and the bosonic a-η' to the infinite volume limit and then to the chiral limit. The extrapolation to the infinite volume was done by fitting the shift $\Delta m(L)$ in the infinite volume mass m_0 due to the finite lattice extend L,

$$\Delta m(L) \simeq C L^{-1} \exp\left(\alpha m_0 L\right) \;, \tag{6.9}$$

with parameters C and $1 \leq \alpha \leq \sqrt{3}/2$. This relation applies to the masses of the stable bound states in a confining theory, therefore also to $\mathcal{N}$=1 SYM, and is independent of the specific form of the interactions. The constants for the glueballs in lattice gauge theory are

$$C = -\frac{3}{16\pi}\frac{\lambda^2}{m_0^2} \quad , \quad \alpha = \frac{\sqrt{3}}{2} \;, \tag{6.10}$$

where λ is the three-glueball coupling constant [40].

The validity of (6.9) was confirmed by fitting it to the masses of the gluino-glue and the η' at different lattice volumes at $\kappa = 0.1490$ as seen in figure 6.1. The dimensionless scale $0.5L/r_0$ is the length in femtometers if the Sommer parameter r_0 is set to the experimental value 0.5 fm in QCD. Since (6.9) is valid only for large L, we did a second fit (red. fit) that excludes the smallest volume. The enhancement of the supersymmetry breaking by finite spatial volume decreases quickly and above $L = 1.2r_0/0.5$ the statistical and systematic errors are of the same orders.

The finite-size effect is enhanced near the chiral limit, therefore the behavior of the mass of the gluino-glue particle extrapolated to the infinite volume limit was observed at different values of $(r_0 m_{a-\pi})^2$ away from the chiral limit. We chose the gluino-glue because the most accurate mass was obtained for it. The results are shown in figure 6.2. The results from the largest lattice of volume $32^3 \times 64$ at different values of κ are consistent with the extrapolated values at different values of $(r_0 m_{a-\pi})^2$. In Table 6.1, one can see that the results from the second largest lattices of volume $24^3 \times 48$ is also consistent with the extrapolated values.

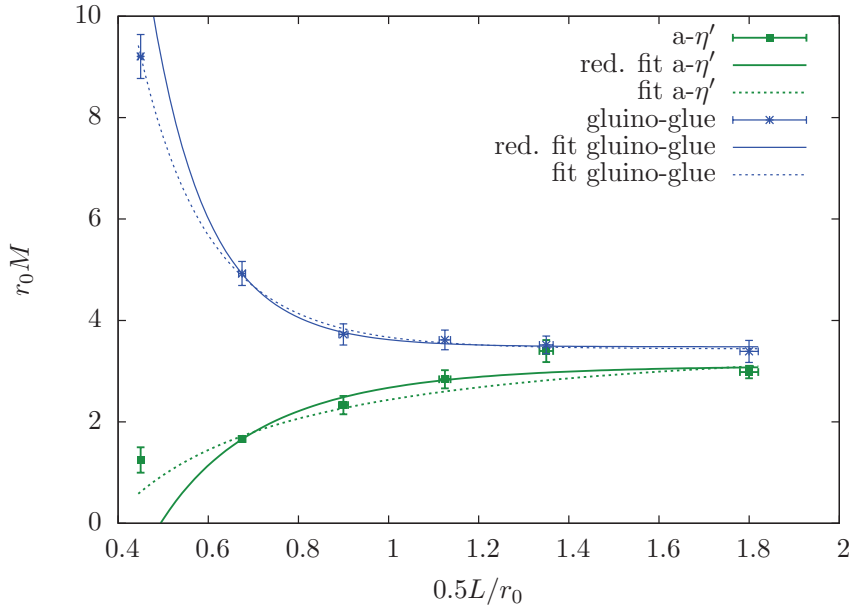

Figure 6.1.: The masses of the gluino-glue and the $a - \eta'$ at different lattice volumes at $\kappa = 0.1490$ and the corresponding fits done using (6.9)

6.3. Mass Spectra

Guided by the results of the analysis on finite-size effects, we used configurations generated on the lattices of volume $24^3 \times 48$ and $24^3 \times 64$ at $\beta = 1.75$ for calculating the masses of the bound states [41]. The configurations were obtained by using a two-step PHMC [42, 43]. We did not include the data from the lattice of size $32^3 \times 64$ because

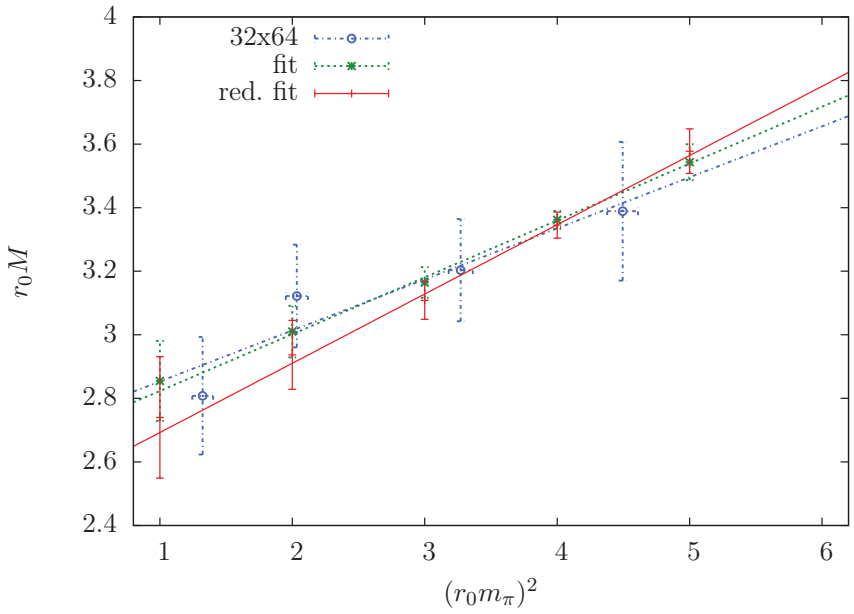

Figure 6.2.: The gluino-glue mass extrapolated to the infinite volume limit as a function of the squared mass of the adjoint pion in units of the Sommer scale and the mass at the largest lattice volume at different values of κ

of low statistics. We applied stout smearing on the links. We have obtained the masses of the gluino-glue, the adjoint mesons and the scalar glueball. We could not get a clear signal for the pseudoscalar glueball. We chosen the values of κ such that $\mathrm{Pf}(M)$ was always positive. Some configurations on the lattice of size $32^3 \times 64$ at $\kappa = 0.1495$ had negative Pfaffian and the methods presented in this thesis were successfully applied on them [44]. But because of low statistics relative to the two other lattices, we did not include data from it in mass extrapolations.

The masses extrapolated to the chiral limit (yellow line) are shown in figures 6.3, 6.4, 6.5 and 6.6. Assuming a linear dependence of the masses on $(r_0 m_\pi)^2$, extrapolation to the chiral limit was done by a linear fit. The best accuracy is obtained for the gluino-glue, as seen in figure 6.3. The masses are almost compatible, suggesting the validity of the prediction of the two degenerate supermultiplets and the existence of a continuum limit with unbroken supersymmetry.

$8^3 \times 16$	$12^3 \times 24$	$16^3 \times 36$	$20^3 \times 40$	$24^3 \times 48$	$32^3 \times 64$	fit	red. fit
9.65(46)	4.51(20)	3.72(34)	2.82(47)	2.48(42)	2.69(23)	2.644(91)	2.47(12)

Table 6.1.: The gluino-glue masses extrapolated to the chiral limit (lower row) at different lattice volumes (upper row). The masses in the last rows were obtained by extrapolating to the chiral limit the masses already extrapolated to the infinite volume limit

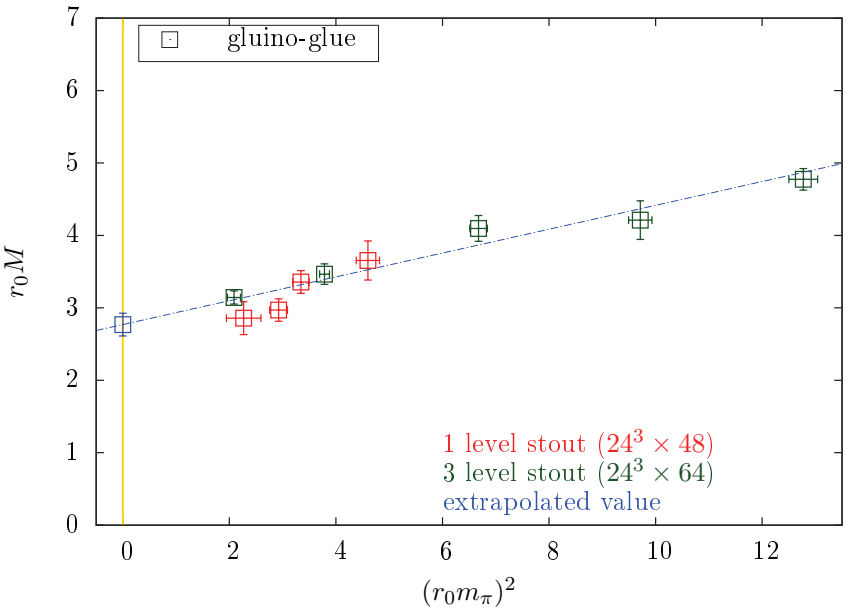

Figure 6.3.: The gluino-glue mass as a function of the squared mass of the adjoint pion in units of the Sommer scale, and the corresponding linear fit

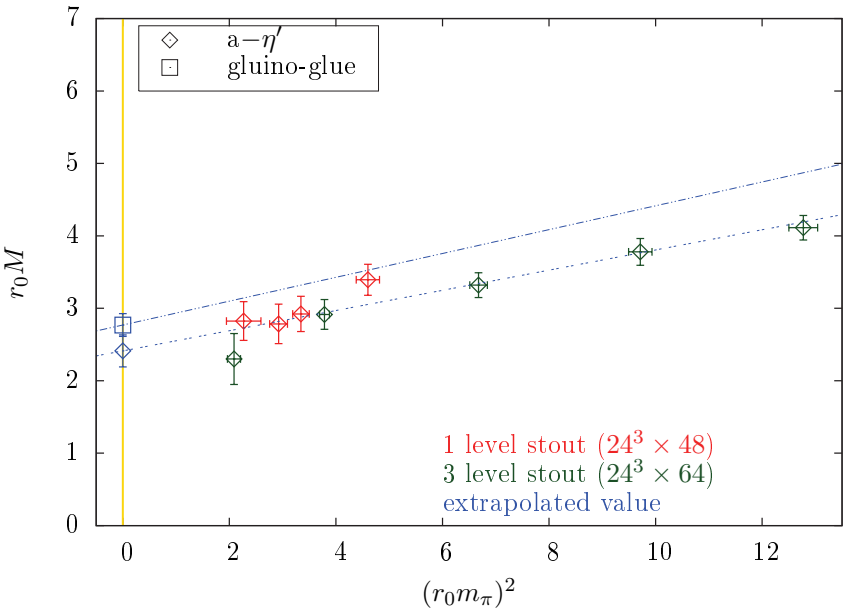

Figure 6.4.: The $a - \eta'$ mass as a function of the squared mass of the adjoint pion in units of the Sommer scale, the corresponding linear fit and the fit for the gluino-glue

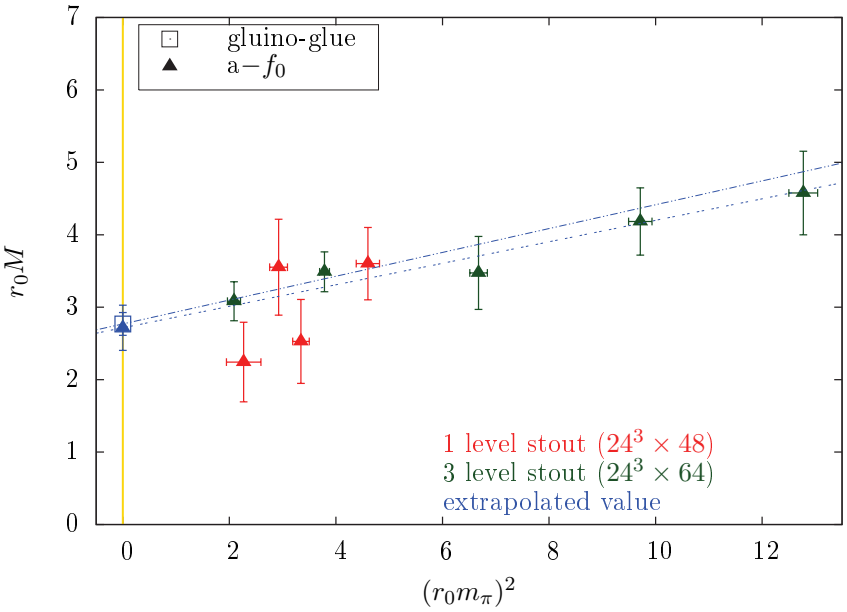

Figure 6.5.: The $a - f_0$ mass as a function of the squared mass of the adjoint pion in units of the Sommer scale, the corresponding linear fit and the fit for the gluino-glue

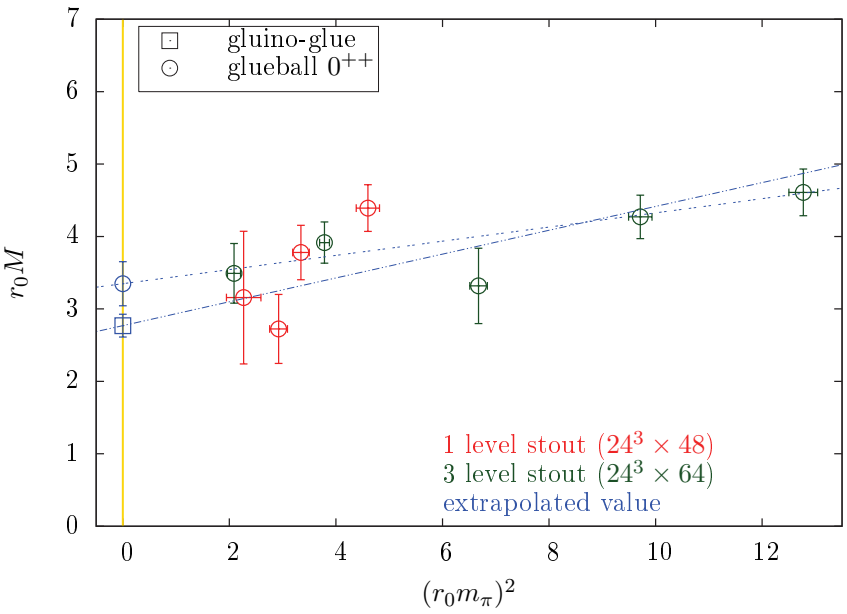

Figure 6.6.: The glueball mass as a function of the squared mass of the adjoint pion in units of the Sommer scale, the corresponding linear fit and the fit for the gluino-glue

7. Conclusion

The sign of the Pfaffian of M needed as a reweighting factor in Monte Carlo simulations of $\mathcal{N}$=1 SYM can be obtained by counting the two-fold degenerate pairs of negative real eigenvalues of D. Preconditioning of D by power polynomials to enable faster and prior access to these eigenvalues were already investigated as an alternative to the spectral flow method. We introduced in this thesis Faber polynomials as a viable alternative to power polynomials. These polynomials were extensively studied in two separate contexts, namely linear systems of equations and numerical conformal mapping. We tried to use this knowledge for lattice simulations. We tested Faber polynomials generated by two types of conformal mappings, the Schwarz-Christoffel mapping and the bratwurst mapping. Use of Schwarz-Christoffel mapping brings much more flexibility in designing a boundary enclosing the region in the complex plane where the uninteresting eigenvalues are predicted to lie. Although this method is prone to numerical instabilities, at least with the tools that we used, it yields considerably high acceleration in eigenvalue extraction. Bratwurst-shaped boundaries are not very flexible and in our tests the Faber polynomials corresponding to the enclosed region in the complex plane containing the uninteresting eigenvalues did not provide acceptable acceleration in eigenvalue extraction. However, their shifted forms resulted in significant acceleration, comparable to that of the most optimal power polynomial that we have. These tests were done at κ values which do not cause too many eigenvalues with a negative imaginary part. Therefore acceleration effects may differ at higher values of κ.

A. Gamma Matrices

In the Weyl representation in Euclidean spacetime, the γ-matrices are

$$\gamma_0 = \begin{pmatrix} 0 & \mathrm{I} \\ \mathrm{I} & 0 \end{pmatrix}, \quad \gamma_{1,2,3} = \begin{pmatrix} 0 & -\mathrm{i}\sigma_{1,2,3} \\ \mathrm{i}\sigma_{1,2,3} & 0 \end{pmatrix} , \tag{A.1}$$

with the Pauli matrices

$$\sigma_1 = \begin{pmatrix} 0 & 1 \\ 1 & 0 \end{pmatrix}, \quad \sigma_2 = \begin{pmatrix} 0 & -\mathrm{i} \\ \mathrm{i} & 0 \end{pmatrix}, \quad \sigma_3 = \begin{pmatrix} 1 & 0 \\ 0 & -1 \end{pmatrix} . \tag{A.2}$$

Then we have

$$\gamma_5 = \gamma_0\gamma_1\gamma_2\gamma_3 = \begin{pmatrix} \mathrm{I} & 0 \\ 0 & -\mathrm{I} \end{pmatrix} . \tag{A.3}$$

We define

$$\sigma_{\mu\nu} = \frac{1}{2}[\gamma_\mu, \gamma_\nu] . \tag{A.4}$$

The charge conjugation matrix C is

$$C = -\gamma_2\gamma_0 = \begin{pmatrix} \mathrm{i}\sigma_2 & 0 \\ 0 & -\mathrm{i}\sigma_2 \end{pmatrix} , \tag{A.5}$$

and it satisfies

$$C^{-1} = C^\top = -C . \tag{A.6}$$

B. Adjoint Representation of SU(N)

Let G a Lie group and g its Lie algebra. Let $A \in G$ and $X \in g$, then $e^{\mathrm{i}tX} \in G$. g is a k-dimensional real vector space, that is, the coefficients X_a are real in

$$X = \sum_{i=1}^{k} X_a T_a . \tag{B.1}$$

The adjoint map

$$\mathrm{Ad} : G \to GL(g) \tag{B.2}$$

such that

$$\mathrm{Ad}A(X) = AXA^{-1} \tag{B.3}$$

is the adjoint representation of G. Note that

$$e^{\mathrm{i}tAXA^{-1}} = Ae^{\mathrm{i}tX}A^{-1} \in G, \tag{B.4}$$

therefore $AXA^{-1} \in g$.

The fundamental representation of an element A of the matrix Lie group $SU(N)$ is simply a unitary, invertible $N \times N$ matrix with $\det A = 1$. Its adjoint representation is a $(N^2-1) \times (N^2-1)$ matrix $\Gamma(A)$ with real elements, since it is acting on the Lie algebra of the group, which is an N^2-1 dimensional real vector space spanned by the generators T_a. Through the adjoint map, Γ is defined by

$$AX_aT_aA^{-1} = X'_bT_b = X_a\Gamma_{ab}T_b, \tag{B.5}$$

where $X'_b \in \mathbb{R}$, therefore Γ_{ab} has real elements. (B.5) implies

$$AT_aA^{-1} = \Gamma_{ab}T_b \ . \tag{B.6}$$

Using

$$\mathrm{tr}(T_aT_b) = \frac{1}{2}\delta_{ab} \ , \tag{B.7}$$

we get

$$\mathrm{tr}(AT_aA^{-1}T_d) = \mathrm{tr}(\Gamma_{ab}T_bT_d) = \frac{1}{2}\Gamma_{ad} \ . \tag{B.8}$$

Therefore

$$\Gamma_{ad}(A) = 2 \ \mathrm{tr}(AT_aA^{-1}T_d) \ . \tag{B.9}$$

C. Majorana Fermions

A Dirac spinor and its adjoint are of the form

$$\psi = \begin{pmatrix} \psi_1 \\ \psi_2 \\ \psi_3 \\ \psi_4 \end{pmatrix}, \quad \bar{\psi} = \psi^\dagger\gamma_0 = \left(\psi_3^*, \psi_4^*, \psi_1^*, \psi_2^*\right) \ . \tag{C.1}$$

It charge conjugate is

$$\psi_c \equiv C\bar{\psi}^T = \begin{pmatrix} \psi_4^* \\ -\psi_3^* \\ -\psi_2^* \\ \psi_1^* \end{pmatrix} \ . \tag{C.2}$$

Majorana spinors λ obey the reality condition $\lambda_c = \lambda$. Therefore they are of the form

$$\lambda = \begin{pmatrix} \lambda_4^* \\ -\lambda_3^* \\ \lambda_3 \\ \lambda_4 \end{pmatrix} . \tag{C.3}$$

with half as many degrees of freedom as Dirac spinors.

Moreover, in terms of Weyl spinors, they are of the form

$$\lambda = \begin{pmatrix} \phi \\ \chi \end{pmatrix} = \begin{pmatrix} \mathrm{i}\sigma^2\chi^* \\ \chi \end{pmatrix} = \begin{pmatrix} \phi \\ -\mathrm{i}\sigma^2\phi^* \end{pmatrix} , \tag{C.4}$$

with

$$\phi = \begin{pmatrix} \lambda_1 \\ \lambda_2 \end{pmatrix} = -\mathrm{i}\sigma^2\chi^* \tag{C.5}$$

and

$$\chi = \begin{pmatrix} \lambda_3 \\ \lambda_4 \end{pmatrix} = -\mathrm{i}\sigma^2\phi^* . \tag{C.6}$$

Bibliography

[1] G. Curci and G. Veneziano, "Supersymmetry and the Lattice: A Reconciliation?," *Nucl.Phys.* **B292** (1987) 555.

[2] R. G. Edwards, U. M. Heller, and R. Narayanan, "Spectral flow, chiral condensate and topology in lattice QCD," *Nucl.Phys.* **B535** (1998) 403–422, `arXiv:hep-lat/9802016 [hep-lat]`.

[3] H. Miyazawa, "Baryon Number Changing Currents," *Prog.Theor.Phys.* **36** (1966) 1266–1276.

[4] Y. Golfand and E. Likhtman, "Extension of the Algebra of Poincare Group Generators and Violation of p Invariance," *JETP Lett.* **13** (1971) 323–326.

[5] A. Neveu and J. Schwarz, "Factorizable dual model of pions," *Nucl.Phys.* **B31** (1971) 86–112.

[6] J. Cornwell, *Group Theory in Physics. Vol. 3: Supersymmetries and Infinite Dimensinal Algebras*. Academic Press, 1989.

[7] V. Ogievetsky and L. Mezincescu, "Symmetries Between Bosons and Fermions and Superfields," *Sov.Phys.Usp.* **18** (1975) 960–982.

[8] R. Haag, J. T. Lopuszanski, and M. Sohnius, "All Possible Generators of Supersymmetries of the S-Matrix," *Nucl.Phys.* **B88** (1975) 257.

[9] S. Ferrara and B. Zumino, "Supergauge Invariant Yang-Mills Theories," *Nucl.Phys.* **B79** (1974) 413.

[10] I. Montvay, "Supersymmetric Yang-Mills theory on the lattice," *Int.J.Mod.Phys.* **A17** (2002) 2377–2412, `arXiv:hep-lat/0112007 [hep-lat]`.

[11] G. Veneziano and S. Yankielowicz, "An Effective Lagrangian for the Pure N=1 Supersymmetric Yang-Mills Theory," *Phys.Lett.* **B113** (1982) 231.

[12] G. Farrar, G. Gabadadze, and M. Schwetz, "On the effective action of N=1 supersymmetric Yang-Mills theory," *Phys.Rev.* **D58** (1998) 015009, `arXiv:hep-th/9711166 [hep-th]`.

[13] J. Gates, S. James, "Super p-form gauge superfields," *Nucl.Phys.* **B184** (1981) 381.

[14] G. Bergner, P. Giudice, I. Montvay, G. Münster, U. D. Özugurel, *et al.*, "Latest lattice results of N=1 supersymmetric Yang-Mills theory with some topological insights," *PoS* **LATTICE2014** (2014) 273, `arXiv:1411.1746 [hep-lat]`.

[15] F. Farchioni, C. Gebert, I. Montvay, and L. Scorzato, "Numerical simulation tests with light dynamical quarks," *Eur.Phys.J.* **C26** (2002) 237–251, `arXiv:hep-lat/0206008 [hep-lat]`.

[16] **DESY-Münster Collaboration** Collaboration, I. Campos *et al.*, "Monte Carlo simulation of SU(2) Yang-Mills theory with light gluinos," *Eur.Phys.J.* **C11** (1999) 507–527, `arXiv:hep-lat/9903014 [hep-lat]`.

[17] R. B. Lehoucq, D. C. Sorensen, and C. Yang, *ARPACK users' guide: solution of large-scale eigenvalue problems with implicitly restarted Arnoldi methods*, vol. 6. Society for Industrial and Applied Mathematics, 1998.

[18] W. E. Arnoldi, "The principle of minimized iterations in the solution of the matrix eigenvalue problem," *Q.Appl.Math.* **9** (1951) 17–29.

[19] C. Gattringer and I. Hip, "Analyzing the spectrum of general, nonHermitian Dirac operators," *Nucl.Phys.Proc.Suppl.* **73** (1999) 871–873, `arXiv:hep-lat/9809020 [hep-lat]`.

[20] Y. Saad, *Numerical Methods for Large Eigenvalue Problems: Revised Edition.* Classics in Applied Mathematics. Society for Industrial and Applied Mathematics, 2011.

[21] H. Neff, "Efficient computation of low lying eigenmodes of non-Hermitian Wilson-Dirac type matrices," *Nucl.Phys.Proc.Suppl.* **106** (2002) 1055–1057, `arXiv:hep-lat/0110076 [hep-lat]`.

[22] J. Wuilloud, *The Wilson-Dirac Operator Eigenspectrum for the Theories of QCD and Super Yang-Mills with One Flavour.* PhD thesis, University of Münster, 2010.

[23] G. Bergner and J. Wuilloud, "Acceleration of the Arnoldi method and real eigenvalues of the non-Hermitian Wilson-Dirac operator," *Comput.Phys.Commun.* **183** (2012) 299–304, `arXiv:1104.1363 [hep-lat]`.

[24] G. Faber, "Über polynomische Entwickelungen," *Math.Ann.* **57** (1903) 389–408.

[25] T. Kövari and C. Pommerenke, "On Faber polynomials and Faber expansions," *Math.Z.* **99** (1967) 193–206.

[26] M. Eiermann, "On semiiterative methods generated by Faber polynomials," *Numer.Math.* **56** (1989) 139–156.

[27] G. Starke and R. S. Varga, "A hybrid Arnoldi-Faber iterative method for nonsymmetric systems of linear equations," *Numer.Math.* **64** (1993) 213–240.

[28] T. Koch and J. Liesen, "The conformal 'bratwurst' maps and associated Faber polynomials," *Numer.Math.* **86** (2000) 173–191.

[29] G. Elliott, *The Construction of Chebyshev Approximations in the Complex Plane*. PhD thesis, University of London, 1978.

[30] S. Ellacott, "Computation of Faber series with application to numerical polynomial approximation in the complex plane," *Math.Comput.* **40** (1983) 575–587.

[31] J. P. Coleman and R. A. Smith, "The Faber polynomials for circular sectors," *Math.Comput.* **49** (1987) 231–241.

[32] J. P. Coleman and N. J. Myers, "The Faber polynomials for annular sectors," *Math.Comput.* **64** (1995) 181–203.

[33] T. Driscoll and L. Trefethen, *Schwarz-Christoffel Mapping*. Cambridge Monographs on Applied and Computational Mathematics. Cambridge University Press, 2002.

[34] L. Trefethen, *Numerical conformal mapping*. J.Comput.Appl.Math. North-Holland, 1986.

[35] T. A. Driscoll, "Algorithm 756: A matlab toolbox for schwarz-christoffel mapping," *ACM T.Math. Software* **22** (1996) 168–186.

[36] T. A. Driscoll, "Algorithm 843: improvements to the schwarz-christoffel toolbox for matlab," *ACM T.Math. Software* **31** (2005) 239–251.

[37] A. Donini, M. Guagnelli, P. Hernandez, and A. Vladikas, "Towards N=1 superYang-Mills on the lattice," *Nucl.Phys.* **B523** (1998) 529–552, `arXiv:hep-lat/9710065 [hep-lat]`.

[38] G. S. Bali, S. Collins, and A. Schafer, "Effective noise reduction techniques for disconnected loops in Lattice QCD," *Comput.Phys.Commun.* **181** (2010) 1570–1583, `arXiv:0910.3970 [hep-lat]`.

[39] G. Bergner, T. Berheide, G. Münster, U. D. Özugurel, D. Sandbrink, *et al.*, "The gluino-glue particle and finite size effects in supersymmetric Yang-Mills theory," *JHEP* **1209** (2012) 108, `arXiv:1206.2341 [hep-lat]`.

[40] G. Münster, "The Size of Finite Size Effects in Lattice Gauge Theories," *Nucl.Phys.* **B249** (1985) 659.

[41] G. Bergner, I. Montvay, G. Münster, U. D. Özugurel, and D. Sandbrink, "Towards the spectrum of low-lying particles in supersymmetric Yang-Mills theory," *JHEP* **1311** (2013) 061, `arXiv:1304.2168 [hep-lat]`.

[42] K. Demmouche, F. Farchioni, A. Ferling, I. Montvay, G. Münster, *et al.*, "Simulation of 4d N=1 supersymmetric Yang-Mills theory with Symanzik improved gauge action and stout smearing," *Eur.Phys.J.* **C69** (2010) 147–157, arXiv:1003.2073 [hep-lat].

[43] I. Montvay and E. Scholz, "Updating algorithms with multi-step stochastic correction," *Phys.Lett.* **B623** (2005) 73–79, arXiv:hep-lat/0506006 [hep-lat].

[44] G. Bergner, G. Münster, D. Sandbrink, U. D. Özugurel, and I. Montvay, "Supersymmetric Yang-Mills theory: A step towards the continuum," *PoS* **LATTICE2011** (2011) 055.

Acknowledgements

I am grateful to Prof. G. Münster for giving me the chance to be a student of his. Every meeting that we had turned into a mini-lecture where he explained obscure concepts using simple examples. I thank Dr. Federico Farchioni for answering every question that I had in the first year of my doctoral studies. A special thank goes to Dr. Georg Bergner. All the tests and results presented in this thesis were possible thanks to a very active collaboration with him, his highly efficient and versatile simulation program and his deep knowledge on a variety of research fields. I had the luck to have Stafano Piemonte as an office mate. I benefited from his expertise in quantum field theory and Mathematica. Dr. Pietro Giudice helped me to understand several concepts in quantum field theory by turning every simple question into a long discussion session. I thank Dirk Sandbrink for his help with computer-related problems. I thank Kai Sparenberg and Michael Holl for answering all my questions on abstract mathematics and Florian König for checking parts of this thesis for errors and ambiguities.

Hiermit versichere ich, die vorliegende Arbeit angefertigt und keine anderen als die angegebenen Hilfsmittel verwendet zu haben.

Münster, den